Title page:

LRBA balances antigen presentation and T-cell responses by facilitating autophagy through the binding to PIK3R4 and FYCO1

Running title: LRBA balances T-cell responses *via* autophagy

Laura Gámez-Díaz[1+], Laura-Anne Ligeon[2*], Elena Sindram[1,3,4*], Marie-Celine Deau[1*], Pablo Sanchez-Martin[5,6], Sigrun Nestel[7], Sophie Jung[1,8], Stefanie Ruf[9], Pankaj Mishra[10], Michele Proietti[1,11,12], Stefan Günther[10], Kathrin Thedieck[9,13,14], Eleni Roussa[7] , Angelika Rambold[1,15], Christian Münz[2], Claudine Kraft [5,6] and Bodo Grimbacher[1,12,16, 17+]

[1]Institute for Immunodeficiency, Center for Chronic Immunodeficiency (CCI), Medical Center – University of Freiburg, Faculty of Medicine, University of Freiburg, Freiburg, Germany.

[2]Viral Immunobiology, Institute of Experimental Immunology, University of Zürich, Zürich, Switzerland

[3]Spemann Graduate School of Biology and Medicine (SGBM), Universtiy of Freiburg, Freiburg, Germany

[4]Faculty of Biology, University of Freiburg, Freiburg, Germany.

[5]CIBSS - Centre for Integrative Biological Signalling Studies, Albert-Ludwigs-University of Freiburg, Freiburg, Germany.

[6]Institute of Biochemistry and Molecular Biology, ZBMZ, Faculty of Medicine, University of Freiburg, 79104, Freiburg, Germany.

[7]Institute of Anatomy and Cell Biology Department of Neuroanatomy, Albert-Ludwigs University of Freiburg, Freiburg, Germany.

[8]Faculté de Chirurgie Dentaire, Université de Strasbourg - Pôle de Médecine et de Chirurgie Bucco-Dentaires, Hôpitaux Universitaires de Strasbourg - Strasbourg, France.

[9]Laboratory of Pediatrics, Section Systems Medicine of Metabolism and Signaling, University of Groningen, University Medical Center Groningen, 9713 AV Groningen, The Netherlands.

[10]Research group of Pharmaceutical Bioinformatics, Institute of Pharmaceutical Sciences, University of Freiburg, Freiburg, Germany.

[11]Department of Rheumatology and Immunology, Hannover Medical School, Hannover, Germany.

[12]RESIST – Cluster of Excellence 2155 to Hanover Medical School, Satellite Center Freiburg, Germany.

[13]Department for Neuroscience, School of Medicine and Health Sciences, Carl von Ossietzky University Oldenburg, 26129 Oldenburg, Germany.

[14]Institute of Biochemistry and Center for Molecular Biosciences Innsbruck, University of Innsbruck, Innsbruck, Austria.

[15]Department of Developmental Immunology, Max Planck Institute of Immunobiology and Epigenetics, Freiburg, Germany.

[16]Clinic of Rheumatology and Clinical Immunology, Center for Chronic Immunodeficiency (CCI), Medical Center – University of Freiburg, Faculty of Medicine, University of Freiburg, Freiburg, Germany.
[17]DZFI – German Center for Infection Research, Satellite Center Freiburg, Germany.

*****These authors contributed equally to this work.

+Corresponding authors:
Laura Gámez-Díaz, laura.gamez@uniklinik-freiburg.de, +4976127077742
Bodo Grimbacher, bodo.grimbacher@uniklinik-freiburg.de, +49127077731

Key points:

- LRBA is required for the different steps of autophagy from autophagosome formation to cargo degradation through the interaction with PIK3R4 and FYCO1.
- Loss of LRBA enhances T-cell driven proinflammatory response as a consequence of increased antigen presentation.

Abstract

Patients with lipopolysaccharide responsive beige-like anchor protein (LRBA) deficiency have an exacerbated T-cell activation and a defective B-cell response. Previously, we suggested reduced autophagy as the biological cause of the aberrant humoral response; however, the exact molecular mechanism of LRBA in autophagy and its impact on T-cell responses remain unknown. We screened for LRBA-interacting proteins, finding that LRBA interacts with the phosphoinositide 3-kinase regulatory subunit 4 (PIK3R4) and with the FYVE And Coiled-Coil Domain Autophagy Adaptor 1 (FYCO1). Interestingly, both proteins play essential roles at different stages of autophagy. Specifically, PIK3R4 facilitates the production of phosphatidylinositol-3 phosphate (PI(3)P) required for the recruitment of PI(3)P-binding adaptor proteins allowing autophagosome formation and autophagosome-lysosome fusion, whereas FYCO1 allows autophagosome movement. LRBA-KO cells showed an impaired production of PI(3)P, a delayed autophagosome-lysosome fusion, an accumulation of abnormal autophagosomes and an atypical lysosomal positioning. These observations explain the decreased cargo material degradation and the overall defective autophagy flux in LRBA-KO cells. Abnormal autophagosomes in LRBA-KO cells are associated with prolonged antigen presentation to T cells, resulting in a higher production of proinflammatory cytokines, as autophagy is a major intracellular degradation system for major histocompatibility class II complex (MHCII) loading. Taken together, our data suggest that i) LRBA forms different protein complexes serving at different stages of autophagy, and ii) loss of LRBA impacts the targeting of cytosolic antigens for autophagy degradation, enhancing antigen presentation. The latter could contribute to the exacerbated T-cell immune dysregulation observed in LRBA-deficient patients.

Introduction

LRBA (lipopolysaccharide responsive beige-like anchor protein*)* belongs to the BEACH-domain-containing protein (BDCP) family that operate as scaffolds for protein interactions and to participate in vesicle trafficking and receptor signalling [1]. Mutations in human BDCPs are associated with various clinical syndromes, five of which directly affect the immune system [1-4]. Among them, a primary immunodeficiency and immune dysregulation syndrome known as LRBA deficiency is caused by biallelic mutations in *LRBA* that abolish its protein expression [5]. Patients with LRBA deficiency display a broad spectrum of clinical manifestations ranging from immunodeficiency, including hypogammaglobulinemia and recurrent infections, to T cell-driven autoinflammation and autoimmunity [6-9]. The latter is thought to be caused by reduced CTLA-4 (cytotoxic T-lymphocyte-associated protein 4) expression on LRBA-deficient activated conventional T cells (Tc) and regulatory T cells (Tregs) due to defective CTLA-4 recycling orchestrated by its direct interaction with LRBA [10]. Therefore, an overlap of the clinical picture of both LRBA deficiency and CTLA-4 insufficiency is frequently observed [11, 12]. However, this solely mechanism (CTLA-4 trafficking alterations) does not explain i) the increased disease severity and mortality and ii) the earlier onset of symptoms observed in LRBA deficient patients as compared to patients with CTLA-4 insufficiency. In fact, we have previously reported that B-lymphocytes from LRBA-deficient patients exhibit defective macroautophagy (hereafter referred as autophagy) under serum deprivation leading to increased apoptosis and reduced plasmablasts survival thereby explaining poor humoral response [5].

Autophagy is a conserved intracellular degradation process where cytoplasmic material such as aberrant/long-lived proteins, intracellular pathogens, and damaged organelles are engulfed in double-membrane vesicles known as autophagosomes, which subsequently fuse with lysosomes for cargo degradation [13]. Although autophagy is a constitutively active housekeeping mechanism that promotes cell survival, it is also essential for modulating several immune system components such as chemokines release upon antigen presentation restricted to the major histocompatibility complex class II complex (MHCII) [14-16]. However, up to date, the molecular mechanism of LRBA in autophagy and the impact of LRBA loss in autophagy-dependent immune functions remain largely unknown.

In the present study, we identified the role of LRBA at early and late stages of the autophagy process through its physical interaction with PIK3R4 (phosphoinositide 3-kinase regulatory subunit 4) and FYCO1 (FYVE And Coiled-Coil Domain Autophagy Adaptor 1). On the one hand, PIK3R4 is the regulatory subunit of the PI3K-complex III that positively regulates autophagy through the

formation of phosphatidylinositol-3-phosphate-PI(3)P, which is needed for the formation of autophagosomes (known as omegasome) and for their fusion with lysosomes [17]. On the other hand, FYCO1 functions as an adapter protein linking autophagosomes to microtubule plus-end-directed molecular motors, which after binding PI(3)P allows autophagosome movement [18, 19]. Here, we show that through these two interactions, LRBA regulates the production of PI(3)P, as well as the size and movement of autophagosomes, autophagosome/lysosome fusion, as well as cargo degradation during autophagy. We also show that LRBA is essential for controlling MHC class II-restricted antigen presentation – an autophagy dependent mechanism – thereby regulating T cell proinflammatory cytokines release. In summary, we identified a novel function of LRBA that is crucial for the immune regulation through the interaction with components of the autophagy machinery.

Material and Methods

Human lymphoblastoid B cell line generation

EBV-immortalized *in vitro* human B cells (LCL) also known as lymphoblastoid B cell line were generated as follows. B cells from three healthy donors (HD) and four LRBA-deficient patients (P1: c.2004+2A>G; P2: p.S2713Hfs; P3: p.Q473*p.E945Efs*; and P4: p.I2646L) were isolated from PBMCs by negative selection using conjugated beads with antibodies against CD2, CD14, CD16, CD36, CD43, and CD235a, according to the manufacturer´s instructions (Miltenyl). Purified B cells were seeded in a 48 well-plate, mixed 1:1 with Epstein-Barr virus (EBV) supernatant, and incubated for four days. Cells were then split and passaged routinely every 3 days in complete RPMI medium (Gibco) containing 10% FCS (Gibco) and 1% Penicillin/Streptomycin (Sigma Aldrich). EBV transformed B cells actively proliferate, secrete antibodies and express LRBA.

Generation of a LRBA knock-out (KO) HEK293T cell line and a HaCat cell line by CRISPR-Cas9 and a LRBA knock-down HeLa cell line by shRNA (shLRBA cells)

LRBA-KO HEK293T cells were generated using the Alt-R-CRISPR-Cas9 system (that includes a crRNA:tracrRNA complex) according to the manufacturer´s instructions (www.idtdna.com). The following gRNA: CCACCAACAGGTGATGACGG is specific for exon 2 of human LRBA, and it was inserted into the cells by electroporation together with the crRNA:tracrRNA complex and the Cas9. Following 48 hours incubation, cells were single cell sorted by flow cytometry and incubated until a visible cell population was detected. LRBA-KO clones were screened using Western blot analysis for LRBA expression followed by a mutation confirmation in the *LRBA gene* by sanger sequencing. Stable knockdown of human LRBA was generated by lentiviral transfection with the short hairpin (sh) RNA expressing vector pLKO.1 (SIGMA). Briefly, pLKO.1 plasmids either

containing the shRNA sequence: CCGGGCAGAAGATATTCACAGACATCTCGAGATGTCTGTGAATATCTT-CTGCTTTTTTG (TRCN0000148136, SIGMA) or the scrambled shRNA sequence: CCGGCA-ACAAGATGAAGAGCACCAATTTTT were transfected overnight into 293 LentiX packaging cells (Takoro) along with VSV-G plasmid envelope (Addgene), aiming to generate shLRBA and shControl encoding lentiviruses, respectively. The next day, medium containing lentiviral particles was collected, filtered and incubated with HeLa cells for 24 h. After virus medium removal, infected HeLa cells were treated with 1 µg/ml puromycin for further positive selection.

Mice

Lrba knock-out mice (*Lrba*$^{-/-}$) were kindly provided by Prof. Manfred Kilimann, Max-Planck-Institut für Experimentelle Medizin (MPIEM), Göttingen, Germany. They were generated on a C57BL/6N background by homologous recombination producing a loss-of-protein deletion of exon 4 of *Lrba* (58).

In silico analysis

The LRBA protein interaction candidates were obtained from STRING and FUNCBase databases that provide known and predicted physical and functional protein-protein interactions. Only interactions with high confidence levels (>0.7) were selected from both databases for further validation. Network visualization was performed with the Cytoscape software provided for both databases.

Modelling of the complex of LRBA and PIK3R4/PIK3C3

The structural modelling of the complex of LRBA and PIK3R4 was based on the finding that LRBA interacts via the WD40 domain with PIK3R4 (see results section). The 3D structure of the WD40 domain was modelled by homology modelling applying the structure of the homolog prokaryotic protein PkwA from Thermomonospora curvata (PDB-ID: 5YZV (ref: PMID: 30154510)). Sequence identity was 26% (39% shared similar residues). Since the first repeat sequence of the WD40-propeller of human LRBA is separated from the other WD40-repeats in sequence, this part of the domain was modelled based on a template of a single propeller and merged with the others, forming a full WD40 propeller domain. For the merging, a WD40 domain with an inserted propeller was used as a structural template (PDB: 3EWE; ref: PMID: 18974315). For the structural modelling of the complex of PIK3R4 with PIK3C3 the homologous structures of the Phosphatidylinositol 3-kinase VPS34 in complex with serine/threonine-protein kinase VPS15 from Saccharomyces cerevisiae was applied (PDB-ID: 5DFZ). Human PIK3C and the template share a sequence identity of 36% (with 54% similar residues). Human PIK3R4 and VPS15 share a

sequence identity of 33% (50% similar residues). The modelling was performed with the homology modelling software Prime (Schrödinger Suite 2018-1, LLC). For the model of the WD40 domain of PIK3R4 we applied the modelling server WDSPdb 2.0 that accurately identifies WD40 repeats and includes them for the correct assignment of the beta sheets in the structural model (PMID: 25348404). The WD40 domain was then connected with the kinase domain of PIK3R4 and finally energy minimized using the OPLS3 force field provided by the Schrödinger software package. The modelling of the complex of PIK3R4/PIK3C3 and LRBA was performed by applying the docking web server HADDOCK (High Ambiguity Driven Biomolecular DOCKing, version 2.2, ref: PMID: 26410586). As input constraints, the single exposed α-helix of the PIK3R4-WD40 domain (sequence motif: VGPSDD) and the smaller top surface of the WD40 domain of LRBA were defined as interacting regions. The top-ranked cluster with the highest negative Z-score value (-2.0) was selected for further analysis.

Immunoblotting and antibodies

Cells were lysed on ice for 15 mins with RIPA buffer (50 mM Tris, 1 % NP-40, 0.5 % sodium deoxycholate, 100 mM NaCl, 1 mM EDTA, 0.1% SDS) + 1x complete EDTA-free protease inhibitor cocktail (Roche). Lysates were then centrifuged at 16,000 g for 10 min at 4°C. Total protein concentrations were determined by bicinchoninic acid (BCA) Protein Assay (Thermo Fisher Scientific). Protein lysates were size-fractionated by SDS-PAGE and electrotransferred to a PVDF membrane in a wet blotting system for 1.5 h at 45V. After blocking with 5% milk in TBST (20 mM Tris, 150 mM NaCl, 0.1% Tween 20), the membranes were incubated at 4°C with any of the following primary antibodies: anti-AMPK total (Cell Signaling), anti-AMPK (pT172; Cell Signaling), anti-FLAG (Sigma Aldrich), anti-GAPDH (Sigma Aldrich), anti-GFP (Santa Cruz), anti-LC3 (Novus), anti-LRBA (Sigma Aldrich), anti-Myc (Cell Signaling), anti-PIK3R4 (Novus), anti-p62 (Enzo Lifesciences), anti-S6K total (Cell Signaling), anti-S6K70 (pT389; Cell Signaling). After overnight incubation with the primary antibodies, membranes were immunodetected with their corresponding secondary HRP-coupled antibody (Santa Cruz). Membranes were washed and developed with Signal Fire or Signal Fire Plus chemiluminescent substrates (Cell Signaling Technology). Peroxidase activity was detected with the Fusion SL device (Peqlab).

Plasmids

Human LRBA was cloned in seven different fragments into pCIneo FLAG vectors (Promega). These plasmids were kindly provided by Dr. Bernice Lo from the National Institute of Health, Bethesda, USA (10). mCherry-GFP LC3 plasmid was a kind gift from Dr. Ian Gentle from the University of Freiburg, Germany, whereas FYCO1-GFP was kindly provided by Dr. Christian

Behrends from the University of Frankfurt, Germany. Human LRBA full length tagged to Myc-DDK was purchased in Origene (RC17204). pVitro-hygro-N-myc-hVps34/Vps15-C-V5-his-plasmid (Addgene #24055), pEGFP-Atg14L (Addgene #21635) and pEGFO-C1-hUVRAG (Addgene # 24296) were provided by Jonathan Backer (*Yan et al., Biochem J, 2009*), Tamotsu Yoshimiri *(Matasunaga K et al.,Nat Cell Biol, 2009)* and Noburo Mizushima *(Kishi C et al., Mol Biol Cell, 2008)*, respectively. LC3-GFP and MP1-LC3 plasmids were previously generated in the laboratory of Christian Münz (*15*).

Immunoprecipitations

LRBA immunoprecipitation (IP), or flag-tagged LRBA (IP) or GFP (IP) were performed using 200 µg of cell lysates from HEK293T cells and 1 µg of either rabbit anti-LRBA, or mouse anti-FLAG antibody (Sigma Aldrich) or mouse anti-GFP (Santa Cruz). Then, 40 µl of Dynabeads protein G (Thermo Fischer Scientific) were added to the lysate/antibody mix and incubated overnight. Beads were washed with lysis buffer, proteins were eluted with 2% SDS and resuspended in Laemmli buffer. 20 µl of the eluted proteins were separated by SDS-PAGE, blotted and detected as described above.

Proximity Ligation Assay (PLA)

In situ PLA was performed using Duolink kit (Sigma Aldrich) according to the manufacturer´s protocol. EBV-B cells from healthy donors 1 and 2, and Patient 1 and 2 were collected, washed with PBS, and fixed with 4% PFA, 2% saccharose for 15 min on ice. Then, cells were placed on glass slides and permeabilized with 0.1% Triton 100 X for 10 mins at 37˚C. Blocking was performed for 30 mins at 37˚C, followed by incubation with the primary antibodies for 1.5h at 37˚C (the same antibody was used for immunoblotting). Cells were washed 2x in washing buffer and incubated with secondary antibodies that are conjugated with oligonucleotides, PLA probe anti-mouse (or anti-goat) MINUS and PLA probe anti-rabbit PLUS, for 1 h at 37˚C. Ligation of the DNA oligonucleotides and amplification reaction with a DNA polymerase were performed at 37˚C for 30 mins and 1h 40 min, respectively. The amplified product was detected with a confocal microscope (Zeiss LSM700) and signal quantification was performed using Duolink Image Tool (Sigma Aldrich).

Transfection conditions

HEK293T cells were seeded in a 6-well plate, co-transfected with 2µg of one of the seven Flag-tagged-LRBA-fragment plasmids, plus 2 µg of PIK3R4-myc using Lipofectamine 2000 Turbofect (Invitrogen) according to the manufacturer´s protocol. Cells were harvested after 48 h, and lysed on ice for 25 mins in a IP buffer containing 50 mM Tris-HCl pH 6.8, 150 mM NaCl, 0.2% NP-40, 1

mM EDTA, plus 1x complete EDTA-free protease inhibitor cocktail (Roche). Lysates were centrifuged at 16,000 g for 10 mins at 4°C. Supernatants were collected for FLAG (Sigma Aldrich) of GFP immunoprecipitation as described above.

Autophagy induction

Naïve B cells ($CD43^{-}B220^{+}CD3^{-}$) were obtained by negative selection (mouse CD43 Ly-48 MicroBeads; MACS Miltenyi Biotec) from spleens of WT and *Lrba*$^{-/-}$ mice with 95% purity, followed by stimulation with LPS from *Escherichia coli* 055: B5 (20 µg/ml, Sigma-Aldrich) for 3 days in complete RPMI medium (L-glutamine, 10% FCS, 100 µg/mL streptomycin, 100 U/mL penicillin, 10 mM HEPES and 1 mM sodium pyruvate). In addition, LPS-stimulated B cells were treated with 100 nM of Bafilomycin A1 (InvivoGen) for 3 h. Next, cell pellets were either used for LC3-II detection by immunoblotting or for morphology and LRBA cellular localization analysis by electron microscopy. In addition, shControl and shLRBA HeLa cells were seeded at $0.3*10^{6}$ cells in 6 well-plates followed by treatment for 16 h or 24 h with 5 µM of MG132 (InvivoGen) alone or in combination with 100 nM of Bafilomycin A1 for 3 h. HEK293T cells were seeded as $0.3*10^{6}$ cells in 6-wells plate followed by treatment for 4 h with 333 nM of Torin 1 (InvivoGen) alone or in combination with 200 nM of Bafilomycin A1 for 1 h.

Measurement of Phosphatidyl inositol-3 phosphate (PI(3)P)

HEK293T cells were seeded at $3*10^{6}$ cells in 10 cm plates followed by treatment for 4 h with 333 nM of Torin 1 or with 1nM of VPS34-IN. After cell collection, cells lysis and extraction of neutral and acidic lipids, PI(3)P was obtained from the organic phase as described elsewhere (24). Finally, PI(3)P was measured using the PI(3)P Mass ELISA kit (Echelon) according to the manufacturer´s protocol.

Autophagosome and lysosome morphology by fluorescence microscopy

To visualize autophagosomes, HeLa cells were transfected with GFP-LC3 using Lipofectamine 2000 (Invitrogen). Additionally, lysosomes were visualized with LysoTracker Red (Invitrogen), according to the manufacturer's instructions. Live images of autophagosomes and lysosomes were acquired in a humidified and CO_2-supplemented imaging chamber on a Zeiss 780NLO confocal microscope. Autophagosomal size was determined from binary images using the analysis particle module of FIJI, with a particle size from 0 to 20 μm^2. To evaluate the mobility of autophagosomes, time lapse movies of autophagosomes were acquired and individual frames color-coded and projected into one image, using the temporal color-coding module of the Zeiss Zen Black software. Autophagosomes were followed for 25 frames and area and velocity were quantified in pixels.

Autophagolysosome visualization

WT and LRBA-KO HEK293T cells were stably transduced with the mCherry-GFP-LC3 tandem vector (kindly provided by Ian Gentle). The cells were then plated on 12 mm cover slides in a 24-wells plate and then treated 4 h with 100 nM Bafilomycin A1 (Invivogen), 333 nM Torin 1 (Invivogen) or Torin 1+Bafilomycin A1. The cells were then fixed 10 mins with 4% PFA (Sigma Aldrich #158127) and the cover slides were mounted with DuoLink In Situ Mounting Medium with DAPI (Merck). The images were acquired using Zeiss LSM710 or LSM880 confocal microscope. The number of dots per cells was assessed with Image J. The autophagosome size was assessed using Imaris 9.7 (Oxford Instruments). Endogenous LC3 and Lamp2 expression was evaluated in WT and LRBA-KO HEK293T cells using the same stimulation as described above. Cells were then fixed 10 min with 4% PFA (Sigma Aldrich #158127) and treated 5 min with ice-cold methanol and 10 min with 0.1% Triton X-100. After 1 h incubation with the primary antibodies LC3B (Cell signalling and Lamp2 (ThermoFisher), the cells were incubated 45 min with secondary antibodies anti-rabbit-AlexaFluor555 and anti-mouse-AlexaFluor647 (Cell Signaling). The cover slides were mounted with DuoLink In Situ Mounting Medium with DAPI (Merck #DEU82040). The images were acquired using Zeiss LSM710 or LSM880 confocal microscope. The number of dots per cells and colocalization was assessed with Image J. The autophagosome size was assessed using Imaris 9.7 (Oxford Instruments).

DFCP1 and WIPI2 expression

WT and LRBA-KO HEK293T cells were plated on 12 mm cover slides in a 24-wells plate and then treated for 1 h with 50 µM Rapamicin (Invivogen), 333 nM Torin 1(Invivogen), 100n M Wortmannin (Invivogen) or incubated with EBSS medium (Thermo Fisher) for starvation. The cells were then fixed 15 min with 4% PFA (Sigma Aldrich) and permeabilized with 0,05% Saponin (Sigma Aldrich #47036) for 10 min and incubated overnight with primary antibody anti-WIPI2 (Abcam, ab105459) or with anti-DFCP1 (LS-bio). The primary antibody was washed away and the cells incubated with secondary antibody anti-mouse AF647 (Cell Signaling). The cover slides were mounted with DuoLink In Situ Mounting Medium with DAPI (Merck). The images were acquired using Zeiss LSM710 or LSM880 confocal microscope. The number of dots per cells was assessed with Image J.

Preembedding immunoperoxidase and immunogold electron microscopy (EM)

For ultrastructural analysis, unstimulated and LPS-stimulated B cells in suspension from WT and *Lrba*$^{-/-}$ mice were centrifuged at 2800 rpm for 10 min. The pellet was fixed in 0.05% glutaraldehyde and 4% PFA in 0.1M PB (phosphate buffer) for 1 h at room temperature (RT), embedded in agar

and cut onto 100 µm slices using a Vibratome. For double labelling with anti-mouse Lamp1 and anti-rabbit LC3 antibodies, slices were blocked with 20% normal goat serum (NGS) and incubated with anti-Lamp1 and anti LC3 overnight at 4°C. Slices were incubated with biotinylated anti-mouse antibody at 1:100 and with goat anti-rabbit IgG coupled to 1.4 nm gold particles at 1:100 in 2% NGS/ 50 mM TBS (Tris-buffered saline) overnight at 4°C. Slices were postfixed in 1% glutaraldehyde, washed with 25 mM PBS for 15 min and the gold particles were enlarged using the silver enhancement kit HQ-Silver from Nanoprobe. Slices were washed, incubated for 90 min using the ABC Elite Kit and peroxidase was visualized by 3'3-diaminobenzidine (DAB). After washing slices were postfixed with 0.5% OsO_4 for 40 min, treated with 1% uranyl acetate for 35 min, dehydrated in a graded series of ethanol, treated with propylene oxide and embedded in Durcupan resin. Slices were cut into 60 nm ultrathin sections, counterstained with lead citrate (according to Reynolds) and viewed in a Zeiss LEO 906 transmission electron microscope. Images were taken using the sharp-eye 2k CCD camera and processed with ImageSP.

LC3B co-localization with HLA-DR molecules in MIICs experiments

$5*10^4$ HaCat cells were seeded in glass cover slips placed inside 24-wells plate and stimulated overnight with IFN-ɣ to induce MHC class II expression. Cells were treated 6 h with 20 µM of chloroquine, and then with 4% paraformaldehyde (PFA) for 15 mins at RT in the dark. Permeabilization was performed with 0.1% Triton X-100 for 5 mins at RT, followed by 3 x PBS washes, cells were saturated with blocking buffer (1% FBS-PBS) for 1h at RT. Primary antibodies were diluted in the blocking buffer and incubated with the cells for 1 h at RT. Primary antibodies used are: rabbit anti-LC3B (MBL), mouse anti-HLA-DR (Cell Signaling). Three PBS washes were performed before staining with Alexa Fluor 488/555-conjugated goat anti-mouse or anti-rabbit (Thermo Fischer) for 1 h at RT. After three PBS washes, cell nuclei were finally stained with DAPI for 5 min prior to mounting the cover slip onto a glass slide using DAKO mounting medium (Agilent). Cells were visualized through 63x, 1.4 NA oil immersion objective with a confocal laser scanning microscope (SP8 upright, Leica) and images were processed with Fiji software.

Membrane flotation assay

Cells from three 15 cm dishes were washed twice with PBS and harvested. The cell pellets were collected after centrifugation at 800 x g for 5 min and resuspended in homogenization buffer (250 mM sucrose, 20 mM Hepes-KOH pH 7.4, 1 mM EDTA and complete EDTA-free protease inhibitor cocktail (Roche)). Cells were lysed by 40 strokes in a glass Dounce homogenizer (WHEATON® Dounce Tissue Grinder). Unbroken cells and debris were removed by two centrifugation steps at 2,000 x g for 5 min. The supernatant was mixed with an equal volume of 50% OptiPrep (D1556-

250ML; Sigma-Aldrich) in homogenization buffer. Discontinuous Optiprep gradients were prepared as described in (Matsui et al., 2018), in SW41 tubes (344059; Beckman Coulter) by overlaying the following Optiprep solutions in homogenization buffer: 2.4 ml of the diluted sample (25% Optiprep), 1.8 ml of 20% Optiprep, 2 ml of 15% Optiprep, 2 ml of 10% Optiprep, 2 ml of 5% Optiprep and 2 ml of homogenization buffer without Optiprep. The gradients were spun at 150,200 x g for 3 h in a SW41 Ti swinging-bucket rotor (Beckman Coulter). 13 fractions of 0.95 ml were collected from the top and subjected to TCA precipitation. The final pellet was resuspended in sample buffer and incubated at 95°C for 5 min.

Proteinase protection assay

Cells treated for 2 h with EBSS and 300 nM Torin 1 were washed with PBS and collected by centrifugation at 500 x g for 5 min. Pellets were resuspended in homogenization buffer (250 mM sucrose, 20 mM Hepes-KOH pH 7.4, 1 mM EDTA and complete EDTA-free protease inhibitor cocktail) and lysed by 30 passages with a 25G needle. After two preclearing steps (2,000 x g, 5 min), cell membranes were pelleted by centrifugation at 20,000 x g for 30 min. The pellet was resuspended in 100 µl of homogenization buffer without EDTA or protease inhibitors, divided into three equal fractions and incubated in the presence or absence of proteinase K (100 µg per ml of sample) with or without 0.5% Triton X-100 for 30 min on ice. The samples were then subjected to TCA precipitation and resuspended in sample buffer.

Statistical analysis

Statistical significance was calculated with a non-parametric two-tailed Mann–Whitney test or t-test using GraphPad Prism 6.0 software. A p value of <0.05 was considered statistically significant (*$p<0.05$; **$p<0.01$; ***$p<0.001$; ****$p<0.0001$).

Results

LRBA interacts with PIK3R4

Members of the BDCP family, including LRBA, have been suggested to act as scaffold proteins interacting and assembling multiple proteins into complexes [1]. Particularly, LRBA interacts with CTLA-4 in T cells; however, LRBA interactors in B cells remain unknown. Hence, we sought to identify additional putative proteins interacting with LRBA using computational predictions based on STRING (search tool for the retrieval of interacting genes/proteins) and FuncBase databases [20, 21]. Computational predictions using both databases generated a total of 28 potential physical or functional interacting partners of LRBA (Figure 1A, left and center, and Table 1). Specifically, FuncBase predicted twenty-one proteins (high confidence defined with score >0.8) and STRING

predicted seven proteins (high confidence defined with score >0.7) to interact with LRBA. Moreover, a Gene Ontology (GO) –term enrichment analysis suggested that the 27 potential LRBA interactors were principally enriched in autophagy and vesicle-trafficking events such as autophagosome formation, assembly and membrane composition, as well as in lysosome organization (Figure 1A, right). Only PIK3R4 (phosphoinositide 3-kinase regulatory subunit 4) was predicted to interact with LRBA by both algorithms (FuncBase and STRING) (Figures 1A, left and center and Table 1). Using proximity ligation assay (PLA) on LCL cells (Lymphoblastoid cell line) from healthy donors (HD) or LRBA-deficient patient (Figure 1B), we validated the physical interaction of LRBA with PIK3R4 at endogenous expression levels. The LRBA-PIK3R4 interaction was further confirmed by co-immunoprecipitation (co-IP) assays from wild type (WT) HEK293T cells transfected with tagged PIK3R4 and LRBA plasmids (Figure 1D). Aiming to determine precisely which LRBA domain interacts with PIK3R4, we performed co-IP experiments using a his-tagged PIK3R4 vector and different LRBA protein domains previously cloned into seven different flag-tagged plasmids (Figure 1E). We identified that the WD40 domain of LRBA (contained in plasmid, so called F3) is required for the interaction with PIK3R4 (Figure 1E-F). Based on these observations, we prepared a structural model of the complex of LRBA and PIK3R4/PIK3C3 by homology modelling. The non-complexed homology model of the WD40 domain of PIK3R4 exhibited one single helix on the surface that was defined as interacting constraints for the docking protocol (Figure 1G). The resulting models of the HADDOCK web server indicated one top-ranked cluster with a high negative Z-score value (-2.0). The best model consisted of a typical WD40 complex in which the exposed α-helix of PIK3R4 interacts with the smaller top surface of the β-propeller via hydrophobic and charged interactions (Figure 1H). A similar binding mode of α-helix recognition has also been observed for some other WD40 domain-containing proteins (*e.g.* PMID: 17392788, PMID: 17227844) [22]. Altogether, our data suggests that the interaction of LRBA with PIK3R4 is a WD40-WD40 interaction.

PIK3R4, also known as Vps15 in yeast, is a 150 kDa protein that is required for the kinase activity of the phosphatidylinositol 3-kinase catalytic subunit type 3 (PIK3C3, or better known as VPS34). Together with Beclin-1, PIK3R4 and VPS34 form the core of the PI3K class III complex (PI3K-III), responsible for the early step of autophagosomes formation [23]. To investigate whether LRBA is part of the PI3K-III complex, we evaluated the interaction of LRBA with VPS34 and Beclin-1 at endogenous and overexpression levels using PLA and co-IP assays. Neither PLA nor co-IP experiments (supplementary Figure 1A-B) supported a physical interaction of LRBA with VPS34 or Beclin-1. The PI3K complex-III core recruits other effector proteins at different autophagy stages, including ATG14L (AuTophaGy Related protein 14L) and UVRAG (UV radiation

resistance-associated gene protein) needed for omegasome formation and autophagosome maturation, respectively [24]. To investigate whether LRBA takes part in any of the complexes formed by PI3K-III complex at the initial steps, we evaluated the interaction of LRBA with ATG14L and UVRAG by co-IP experiments. Our western blot images showed no interaction of LRBA with ATG14L in WT HEK293T cells after co-transfecting LRBA and ATG14L (overexpression system). However, we observed an interaction of LRBA with UVRAG (supplementary Figure 1C and 1D). Moreover, we also evaluated by PLA the proximity of LRBA with phosphatidylinositol 3-kinase delta (PI3K-delta), another member of the PI3K family, which is essential for immunity. Our results show absence of the PLA signal in LCL from a HD, indicating no interaction, nor proximity of LRBA with PI3K-Delta (supplementary Figure 1E). Altogether, these results demonstrate that LRBA interacts specifically with PIK3R4 from the PI3K-III complex, through the WD40 domain, possibly primarily influencing UVRAG containing PI3K-III complexes that are involved in autophagosome maturation.

PI3K complex III activity requires LRBA

The PI3K-III complex plays a pivotal role as a positive regulator of autophagy by generating phosphatidylinositol 3-phosphate (PI(3)P). In turn, PI(3)P allows the recruitment of various PI(3)P-binding effector proteins at early (formation of autophagosome) and late (maturation of autophagosome) stages of autophagy [25, 26] (Figure 2A). Aiming to determine whether LRBA is necessary for a proper PI3K-III complex activity, we first assessed the effect of LRBA loss on the PI(3)P production capacity. We measured the levels of PI(3)P in lipid extracts from LRBA-KO HEK293T cells (generated by CRISPR/Cas9 approach, supplementary Figure 2A-B) and their controls (hereafter known as WT) at steady-state conditions (or basal condition), upon autophagy induction with Torin 1 (an ATP analogue mTORC1), and after PI3K-III complex inhibition with VPS34-IN1 (a specific inhibitor of VPS34, figure 2A). Torin 1 increased the levels of PI(3)P in WT but not in LRBA-KO HEK293T cells after autophagy induction compared to their basal condition. (Figure 2B). Instead, the PI(3)P levels in LRBA-KO cells remained comparable to those upon blockade of VPS34 using VPS34-IN1 (Figure 2B). At early stages of autophagy, PI(3)P recruits double FYVE domain-containing protein-1 (DFCP-1) and WD repeat domain phosphoinositide-interacting protein-2 (WIPI2) to the omegasomes (PI3P-enriched ER sections), which in turn serve as the scaffolds for autophagosomes formation [27, 28] (Figure 2A). To evaluate the effect of the lack of LRBA and the concomitant low production of PI(3)P on the recruitment of these effector proteins, we analyzed the accumulation of DFCP-1 and WIPI2 in WT and LRBA-KO HEK293T cells by fluorescence microscopy. We observed significantly reduced accumulation of both WIPI2

and DFCP-1 in LRBA-KO cells in comparison to the WT counterparts after autophagy induction with Torin 1, Rapamycin or upon serum-deprivation (starvation) (Figure 2C –E). The specificity of the DFCP-1 signal was validated after inhibition of the PI3K-III complex using different concentrations of the VPS34 inhibitor, VPS34-IN1 (Figure 2F-G). All together, these results indicate that LRBA is essential for the proper production of PI(3)P and thereby the recruitment of PI3P-binding effector proteins, DFCP-1 and WIPI2 to the omegasome. These results suggest an abnormal autophagosome biogenesis in the absence of LRBA.

LRBA deficiency results in a blockage of autophagosome-lysosome fusion

We next addressed whether the poor association of WIPI2/DFCP-1 with PI(3)P due to the absence of LRBA affects autophagosome formation and maturation, and ultimately autophagy flux. Therefore, we stably transduced WT and LRBA-KO HEK293T with a mCherry-GFP-LC3 tandem vector, a well-characterized tool to follow autophagosome maturation [29]. With it, autophagosomes are intracellularly visualized as a double positive mCherry and GFP signal (yellow), whereas the autophagolysosomes are observed as a single mCherry (red) signal due to the low-pH-related protonation of the GFP. Both WT and LRBA-KO cells showed no punctate structures at basal condition, consistent with a low autophagy level (Figure 3A-B). Upon autophagy induction with Torin 1, LRBA-KO cells showed a higher GFP signal compared to WT cells (reduced red/green signal), suggesting an accumulation of autophagosomes due to an impairment of the fusion of autophagosomes with lysosomes (Figure 3A-B). These observations were confirmed by studying the conversion of LC3-I into LC3-II in shLRBA HeLa cells (knock-down LRBA, supplementary Figure 2C and 3A-B) and in LPS-stimulated B cells from *Lrba* KO mice in comparison to their WT littermates (supplementary Figure 3E-F). Interestingly, an accumulation of p62 (cargo protein) was observed after autophagy induction in LRBA-KO HEK293T cells (Figure 3C-D) and in shLRBA HeLa cells (Supplementary Figure 3C-D). These observations suggest that loss of LRBA leads to a blockage of the autophagosome-lysosome fusion, reducing the overall autophagy flux evidenced by impeded degradation of p62. Interestingly, our fluorescent microscopy analysis on LC3-transfected HEK293T and HeLa cells also revealed increased autophagosomal size in cells lacking LRBA (Figure 3E and Supplementary Figure 3G). Enlarged LC3-positive autophagosomes were also observed at endogenous LC3 protein levels (Figure 3F-G). Taken together our observations suggest a reduced autophagic flux and a deficient degradation of cargo material due to a blockage of autophagosome-lysosome fusion in the absence of LRBA.

Loss of LRBA leads to abnormal accumulation of enlarged sealed autophagosomes

To analyse whether these enlarged autophagosomes are matured and sealed, we performed a protease protection assay and monitored the sensitivity of p62 to proteinase K treatment by immunoblotting. In this assay, if p62 is enclosed within mature autophagosomes, it is protected from proteinase K activity, whereas degradation of p62 indicates unsealed autophagosomes (Figure 4A). We observed a protease protection of about 25% of total p62 in WT HEK293T cells, whereas LRBA-KO cells showed an increased p62 protease protection of about 50%, suggesting an accumulation of sealed autophagosomes in the absence of LRBA (Figure 4B-C). To verify that LRBA-KO cells accumulate enlarged autophagosomes, we used a membrane flotation method using a stepwise OptiPrep gradient [30]. With this method, unfused autophagosomes have been shown to float at a low density of 5% OptiPrep, whereas other membranes such as autophagic precursor membranes but also mitochondria, ER and lysosomes float at higher densities [30]. Similar to these previous reports, we found non-lipidated LC3-I, which represents soluble proteins, at the bottom of the gradient in fraction 13 (Figure 4D), and LC3-II, which represents membrane-lipidated proteins and marks autophagic precursor membranes, in higher density fractions (F9-F5) of 10-15% OptiPrep in starved and Torin1-treated WT HEK293T cells. Complete autophagosomes rapidly fuse with lysosomes, and therefore are difficult to detect under these conditions. Hence, to enrich for mature autophagosomes, we treated HEK293T cells with Bafilomycin A1 that blocks the fusion of autophagosomes with lysosomes. Under these conditions, LC3-II was found at even lower densities of 5%, as expected and previously reported, indicating the formation of mature autophagosomes (Figure 4D). Interestingly, when analyzing LRBA-KO cells, LC3-II was already found in 5% fractions without Bafilomycin A1 treatment, suggesting that unfused autophagosomes accumulated in these mutant cells (Figure 4D). Similar results were obtained when monitoring the autophagosomal soluble N-ethylmale-imide-sensitive factor-attachment protein receptors (SNARE) protein STX17 (Figure 4D). Accumulation of enlarged autophagosomes was also observed by electron microscopy (EM) after immunogold labelling of LC3 in isolated LPS-stimulated B cells from *Lrba* KO mice (Figure 4E). In WT mice however, autophagosomes were hardly detectable due to their rapid turnover. Taken together our observations show that loss of LRBA leads to abnormal accumulation of enlarged sealed autophagosomes.

Increased mTORC1 signalling in the absence of LRBA

Autophagy is regulated by the mechanistic/mammalian target of rapamycin complex (mTORC1), an evolutionary conserved serine/threonine kinase protein complex, which is composed of the mTOR kinase and the specific scaffold regulatory-associated protein of mTOR (Raptor) [31, 32].

As PI3K-III complex has been suggested to regulate mTORC1, we therefore evaluated the phosphorylation status of mTOR *bona fide* substrate, p70-S6K1 [33]. Hyperphosphorylation of p70-S6K1 was observed in LRBA-deficient LCL cells as well as in shLRBA HeLa cells (Figure 4F-G). Of note, the mTORC1 antagonist AMP-dependent kinase (AMPK) also showed a trend to increased activity, as assessed by phosphorylation at T172 in both cell lines. AMPK inactivates mTORC1 and enhances autophagy [34]. Thus, AMPK may act to sustain residual autophagy compensating for the decreased activity of PI3K complex III in absence of LRBA. Together, these observations suggest a role of LRBA at regulating mTORC1 activation.

Absence of LRBA affects autophagosome mobilization and lysosome positioning

The lack of LRBA leads to an autophagy impairment by modifying the biology and physiology of autophagosomes, which was demonstrated by the accumulation of enlarged autophagosomes that fuse less with lysosomes. Thus, we were wondering whether their mobility would also be affected by the lack of LRBA, explaining the decreased cargo elimination *via* autophagy. Indeed, live-microscopy data on GFP-LC3 transfected HEK293T cells revealed that the enlarged autophagosomes observed in LRBA-KO cells have reduced velocity in comparison to regular sized autophagosomes (Figure 5A-C and supplementary video 1 and 2). Using lysotracker (probe for acidic organelles), we also identified an irregular lysosomal positioning observed as a cytosolic spread-out signal in LRBA-KO cells, in contrast to the perinuclear location observed in WT cells (Figure 5D). However, a comparable expression of endogenous Transcription Factor EB (TFEB) protein was seen in cell lacking LRBA and in WT cells, indicating a normal lysosome biogenesis (Figure 5E). EM imaging showed accumulation of lysosomes in B-lymphocytes from *Lrba* KO mice upon i*n vitro* stimulation with LPS (Figure 5F). Together, these data suggest an additional role of LRBA in the degradation pathways by being involved in the trafficking of autophagosomes and/or lysosomes. To confirm these observations, we searched for another LRBA interaction partner specifically involved in autophagosome and lysosome trafficking, using unbiased IP-MS/MS data previously generated within “The Human Autophagy Interaction Network- AIN” [35]. AIN reported a proteomic analysis of the autophagy interaction network in human cells under basal autophagy, revealing a network of 751 interactions. LRBA was identified within the FYCO1 interactome (http://besra.hms.harvard.edu/ipmsmsdbs/comppass_viewer.php?bait=FYCO1). FYCO1 is a multidomain adaptor protein that mediates microtubule plus-end-directed autophagosome transport by simultaneously interacting with kinesin motor proteins and autophagosomal proteins such as Rab7, microtubule-associated protein 1 light chain 3 (LC3) and PI(3)P [18, 19, 36]. Following co-IP analysis in HEK293T cells co-transfected with GFP-tagged FYCO1 and Myc-

tagged LRBA, we confirmed a physical interaction between LRBA and FYCO1 (Figure 5G). Additional co-IP experiments using the seven different flag-tagged LRBA protein domains and the GFP-tagged FYCO1, identified several potential binding sites contained in plasmids F1, F5 and F6 (Figure 5H). Of note, F6 contains the LRBA PH-BEACH domain, which has been previously reported to interact with the tail of CTLA-4. Altogether, our results show that LRBA interacts with PIK3R4 and FYCO1 under basal autophagy conditions, suggesting a role of LRBA at different stages of autophagy by forming different protein complexes with the molecular machineries of this pathway.

Enhanced T-cell response due to increased MHC class II restricted antigen presentation in LRBA deficiency

Autophagy is a major intracellular degradation system that delivers self and foreign cytoplasmic proteins to lysosomes for further loading onto MHC class II molecules. Peptides bound to MHC II molecules are later transported to the cell membrane for antigen presentation to $CD4^+$ T lymphocytes thereby initiating immune responses [37]. To test whether defective autophagy due to LRBA loss affects MHC class II mediated antigen presentation, we used the Influenza A matrix protein 1 (MP1) directly fused to the autophagic protein LC3 (MP1-LC3), known to strongly enhance its presentation *via* MHC class II to $CD4^+$ T cell clones [15]. Thus, the abilities of WT and LRBA-KO HaCat cells expressing MP1-LC3 (target cell) to activate MP1-specific $CD4^+$ T cell clones (effector cells) were assessed by their cytokines that are secreted in response to this stimulation (Figure 6A). We detected increased secretion of IFN-γ, TNF-α, IL-6 and MIP-1β cytokines in the supernatant of $CD4^+$ T cell co-cultured with LRBA-KO HaCat cells compared to WT HaCat cells (Figure 6B-E). Influenza MP1 antigen specificity was confirmed by the lack or lower secretion of these cytokines by the MP1-specific $CD4^+$ T cell clones when incubated with WT HaCat cells expressing the GFP-LC3 control protein (Figure 6B-E). Thus, the loss of LRBA seems to increase MHC class II antigen presentation through autophagy enhancing $CD4^+$ T cell stimulation. Further confocal microscopy analysis of the MHC class II compartment (MIIC) for antigen loading revealed single HLA-DR or both HLA-DR and LC3 containing vesicles were enlarged in size in LRBA-KO HaCat cells compared to the WT control (Figure 6G-H). In addition, we observed more $HLA\text{-}DR^+$ vesicles and a trend towards increased co-localization with LC3 in LRBA-KO HaCat cells. This suggests an accumulation of autophagosome delivering antigens inside the MIICs of LRBA-deficient cells (Figure 6 G-I). These observations are in line with our findings of enlarged autophagosomes and accumulation of cargo protein p62 in LRBA-KO HEK293T cells. Our data suggest that the lack of LRBA results in increased MHC class II restricted

antigen presentation of autophagy substrates by delaying the maturation and fusion of autophagosomes with lysosomes.

Discussion

In 2012, we suggested that defective autophagy is the cause of increased B cell apoptosis and poor plasma cell differentiation in patients with LRBA deficiency. However, the underlying mechanism of the role of LRBA in the autophagy process had yet to be determined. In this study, we provide evidence that LRBA facilitates autophagy through the interaction with PIK3R4 and FYCO1. Loss of these interactions resulted in low PI(3)P production, enlarged autophagosomes, aberrant trafficking and positioning of autophagosomes and lysosomes, leading to a reduced fusion of autophagosomes with lysosomes and thereby an inefficient degradation of cargo proteins *via* autophagy. Abnormal autophagy resulted in enhanced MHC class II restricted antigen presentation and $CD4^+$ T cell activation in the context of LRBA deficiency.

Our data suggests that LRBA-PIK3R4 interaction occurs *via* WD40-WD40 domain binding. WD40 is one of the most common interacting domains in eukaryotic cells, and it is known to serve as platforms for the assembly of multiprotein complexes, or mediators of transient protein interactions [38]. WD40 domains are characteristically present in BDCP family members like LRBA, allowing them to act as scaffolding proteins, or like WDFY3/ALFY allowing its interaction with PI3K-III to participate in cargo selection and delivery to autophagosomes during selective autophagy [39, 40] [1]. In contrast, WD40 domains are not abundant in PI3K family members. In fact, only PIK3R4 harbours a WD40 domain within this protein family, supporting our findings that LRBA specifically interacts with this protein and not with other PI3K family members, such as PI3K delta [41]. In addition, we showed that LRBA interacts with FYCO1 *via* its BEACH domain, a domain typically involved in vesicle trafficking [1]. In the same line, LRBA is also known to interact with CTLA-4 through its BEACH domain facilitating the trafficking of CTLA-4-containing vesicles in regulatory T cells [10]. These findings indicate that LRBA forms distinct protein complexes through its BEACH and WD40 domains that play a role in both CTLA-4 mobilization and autophagy. However, in view of the different adaptor proteins involved in these interactions, LRBA might also act in additional vesicle trafficking pathways. Future analysis evaluating whether these LRBA protein interactions are cell specific or stimuli specific, need to be performed.

In addition, we observed that the LRBA-PIK3R4 interaction facilitates the production of PI(3)P, as LRBA-KO HEK cells and shLRBA HeLa cells failed to produce PI(3)P after autophagy induction. Interestingly, at resting conditions, both WT and LRBA-KO cells produced equal amounts of PI(3)P

suggesting that the PI(3)P constitutive pool is not affected by the loss of LRBA-PIK3R4 interaction. Indeed, downregulation of VPS34 expression, a key member of the PI3K-III complex, in resting glioblastoma cells, resulted in a residual production of PI(3)P [42]. There, PI(3)P localized mostly to early endosomal membranes and to the internal membranes of multivesicular endosomes. This indicates that the PI(3)P constitutive pool is generated independently of the PI3K-III complex, and that the loss of VPS34 affects specifically late endosomal morphology and function, but not early endosomes morphology and trafficking [42-44]. In addition, VPS34-KO cells have shown normal vesicle trafficking between the trans-Golgi and late endosomes, normal endocytic uptake of fluid-phase markers, and normal association with early endosomes, but disrupted late endosomal trafficking [32]. Therefore, the effect of LRBA in the trafficking of CTLA-4 containing vesicles could also be related to an aberrant activity of the PI3K-III complex. Further analysis of PI(3)P levels in stimulated memory T cells or Tregs of LRBA-deficient patients should be investigated. In addition, we demonstrated here that LRBA interacts with UVRAG. Together with PIK3R4 and VPS34, they form a protein complex located at the membrane of early endosomes with an essential role in endocytosis (including phagocytosis, pinocytosis and internalization of specific receptor-ligand complexes), cytokinesis and lysosome recycling. Hence, we suggest that LRBA might affect other vesicle trafficking processes.

PI(3)P acts as a membrane-bound localized signal. It controls the assembly of protein scaffolds that contain PI(3)P-binding sites to mediate autophagosome biogenesis, maturation, and intracellular transport including endocytosis and phagocytosis [45]. In particular, PI(3)P recruits WIPI2 and DFCP-1 (or ZFYVE1) for omegasome biogenesis. WIPI2 is necessary for the recruitment of the protein complex involved in the lipidation of the phagophore-forming protein LC3B [46, 47] whereas DFCP1 -a recently found ATPase- is necessary for releasing the newly formed autophagosomes from the ER site for selective autophagy (Viola Nähse, ATPase, BioRXiV, preprint 2022, https://doi.org/10.1101/2022.02.24.481614). Our data show that loss of LRBA results in reduced accumulation of both DFCP-1 and WIPI2 upon autophagy induction. However, residual PI(3)P and lower DFCP-1/WIPI-2 recruitment allowed the generation of autophagosomes in the absence of LRBA, resulting in similar levels of LC3 lipidation (LC3-II; Figure 3B). In line with these observations, normal omegasome formation was also observed in DFCP-1-mutant cells (Viola Nähse, ATPase, BioRXiV, preprint 2022, https://doi.org/10.1101/2022.02.24.481614) as well as in Vps34-mutant cells, despite reduction in the puncta number of WIPI-2 [48]. Similar to our observations, shVPS34 glioblastoma cells as well as *vps34*-KO MEF cells showed enlarged late endosome morphology. However, abnormal endosomes from *vps34*-KO had an intact capacity to merge with lysosomes [42]. This observation

contrasts with our data, showing a blockage of autophagosome/lysosome fusion in LRBA-KO cells, which highlights the additional role played by LRBA in the autophagy process. We suggest that LRBA-FYCO1 interaction is essential for autophagosome mobilization and regular lysosomal positioning followed by autophagosome/lysosome fusion. This suggestion is reinforced by previous reports showing the importance of FYCO1 for intracellular transport of autophagic vesicles [49]. Mechanistically, FYCO1 binds to the autophagosomal membrane *via* PI(3)P interaction and to the GTP-bound Rab7 effector protein through its FYVE domain, allowing the tethering of autophagosomes to plus-end-directed microtubule proteins leading to autophagosome movement [18, 19]. FYCO1 has also been involved in the transport and protrusion of other endocytic organelles, lysosomes and phagosomes, which explained the abnormal localization of the lysosome observed in cells lacking LRBA [50, 51]. In addition, depletion of FYCO1 led to accumulation of residual autophagosomes as we observed in LRBA-KO cells [35]. Furthermore, formation of autolysosomes is one of the essential steps for ultimate autophagic degradation, which depends on i) an efficient microtubular migration of mature autophagosomes to the location of lysosomes, and once they encounter, ii) on a tight coordination of several effector proteins that facilitate the fusion of the autophagosomal and lysosomal lipid bilayer membranes, allowing the release of the lysosomal enzyme to degrade the sequestered cargo. Some of these effector proteins including FYCO1, are recruited through binding to PI(3)P at the autophagosome/lysosome membranes [52, 53]. Hence, LRBA is essential for both PI(3)P production and for trafficking and mobilization of autophagosomes/lysosomes, thereby confirming the requirement of LRBA for autophagic flux, in particular autophagosome maturation.

Autophagy is an essential mechanism for multiple immune functions in B and T lymphocytes. In fact, defective autophagy was previously reported by our group in human naïve B cells from LRBA-deficient patients upon serum-deprivation culture conditions [5]. The selective importance of autophagy for plasmablasts survival and differentiation as well as for antibody production has previously been demonstrated in Atg5-deficient mice [54, 55]. In line with these results, LRBA-deficient patients characteristically show low numbers of plasmablasts and low titers of serum immunoglobulins [8]. Moreover, recent studies have also demonstrated the essential role of autophagy for BCR internalization, cytoskeleton polarization, and self-renewal of B1a B cells, a polyspecific-IgM producer B cell subset [56, 57]. Interestingly, *Lrba* KO mice had significantly reduced numbers of B1a B cells in comparison to their WT littermates, suggesting defective autophagy in this cell subset in the absence of LRBA [58]. Further studies showing whether the absence of LRBA affects glycolysis and oxidative phosphorylation in B cells, known to be a key regulator for B1a B cell population renewal, as well as its impacts on BCR internalization and

cytoskeleton polarization, should be addressed. Although abnormal autophagy in LRBA-deficient T cells has not been yet reported, it is known that VPS34-dependent autophagy plays a critical role in maintaining T-cell homeostasis by promoting T-cell survival through the quality control of mitochondria [59], suggesting that LRBA might influence T cell survival. However, LRBA-deficient patients have normal numbers of circulating T cells, indicating that LRBA might not be important for autophagy in the survival of T cells. However, it could have a role in other endocytic trafficking routes similar to the vesicular trafficking of CTLA-4. In addition to immune cell survival and differentiation, autophagy is a key actor during antigen processing for MHC class II restricted presentation to $CD4^+$ T cells, influencing autoimmunity, tumor immunology and immune control of infectious diseases [37]. Mechanistically, self- and non-self-peptides are first processed by autophagy, and then loaded onto MHC class II molecules in MIICs, followed by their transport to the cell membrane for $CD4^+$ T cell stimulation [37]. Based on previous evidence showing that autophagosome-targeted influenza matrix protein 1 (MP1) ed to MHC class II restricted presentation to $CD4^+$ T cells, we evaluated the same response but in the context of LRBA deficiency [15]. Our results showed enlarged vesicles with increased co-localization of LC3 and the MHC class II molecules HLA-DR in LRBA-KO HaCat cells, suggesting an accumulation of autophagy substrates in MIICs. Similar vesicle enlargement and accumulation of the autophagy cargo protein p62 was also observed in LRBA-KO HEK293T and shLRBA HeLa cells, confirming our previous observation that the absence of LRBA led to an accumulation of autophagosomes with delayed maturation. Furthermore, the influenza MP1 specific $CD4^+$ T cell clone co-culture with cells lacking LRBA resulted in increased proinflammatory cytokines secretion, indicating enhanced activation of $CD4^+$ T cells in absence of LRBA. Accumulation of enlarged MIICs allow us to hypothesize that the missing interaction of LRBA and FYCO1 might also block the trafficking of HLA-DR containing vesicles, allowing for prolonged peptide loading onto MHC class II molecules. With time the autophagy delivered peptide repertoire will be processed leading to a prolonged antigen presentation that results in enhanced and chronic T cell activation. These observations are in line with the clinical picture of LRBA-deficient patients, which is characterized by immune dysregulation of the T cell response [6, 8, 9]. Enhanced proinflammatory response in the context of LRBA deficiency has also been reported for *Lrba* KO mice that display increased susceptibility to DSS-induced colitis. The latter has been attributed to abundant production of type I IFN in IRF3/IRF7- and PIK/mTOR-dependent manners in dendritic cells, thus recognizing a role of LRBA in the endolysosomal pathway to limit TLR signalling [60].

mTORC1 is activated in response to growth factors, nutrients and antigen binding to enhance biosynthetic processes while inhibiting catabolic processes such as autophagy. In contrast, AMPK activates the initial steps of autophagy and thus acts in an antagonistic manner to mTORC1 [61,

62]. Here, we show that LRBA-deficient LCL cells exhibit concomitant high mTORC1 and AMPK activity, which has been reported earlier under nutrient sufficiency [63]. While high mTORC1 signalling might contribute to defective autophagy in the context of LRBA deficiency, AMPK may act to sustain residual autophagy. Thus, inhibitors of mTORC1 such as rapalogs, or activators of AMPK such as metformin, may be valuable treatment options for LRBA-deficient patients, as both types of compounds are clinically approved for other diseases (*e.g.* cancer and diabetes), and exhibit acceptable toxicity profiles [64, 65]. In fact, several clinical reports on patients with LRBA deficiency demonstrated that treatment with sirolimus, a mTOR inhibitor, led to improvement of their clinical symptoms, especially enteropathy [8, 66, 67].

In conclusion, we propose a role of LRBA as a scaffold protein required at early and late stages of autophagy process through the interaction with PIK3R4 and FYCO1, two novel interactors of LRBA in human cells. PIK3R4-LRBA and FYCO1-LRBA interactions are essential to facilitate the proper production of PI(3)P upon autophagy induction, as well as the formation of autolysosomes required for the degradation of the sequestered cargo material. Through this mechanism, LRBA regulates MHC class II restricted antigen presentation and T-cell mediated responses. In the absence of LRBA, cells can form autophagosomes but autophagic flux is impaired due to a blockade of autophagosomes-lysosomes fusion that leads to defects in size, frequency and movement of autophagosomes. Accumulation of cargo/antigenic peptides, particularly in the same vesicles that contain MHC class II molecules, results in enhanced antigen presentation leading to a stronger proinflammatory immune response.

Acknowledgements

We thank Dr. Bernice Lo (National Institute of Allergy and Infectious Diseases, Bethesda, USA), Dr. Christian Behrends (University of Frankfurt, Germany) and Dr. Ian Gentle (University of Freiburg, Germany) for kindly providing us with plasmids. We thank Dr. Michael Moutschen (University of Liege, Belgium) and Prof. Manfred Kilimann (University of Gottingen, Germany) for kindly sharing with us the shLRBA HeLa cell line and the *Lrba-ko* mice, respectively, which were previously generated at their laboratories. In addition, we thank Jessica Rojas-Restrepo, Hanna Haberstroh, Türkan Güzel, Katja Malfertheiner, Vanessa Zeidler and Julika Neumann from our research group for their technical assistance during these past years, and to Dr. Virginia Andreani for her thorough review of this manuscript. We thank Dr. Marie Follo from the Light Core Facility Unit for her support and teaching of the microscopes. Schematic illustrations were created using Biorender licenses # QO24HLH0U1 and #KZ24HLGTRC. This study was supported by the Fritz Thyssen Foundation (grant number: 10.18.1.039MN), the Bundesministerium für Bildung und

Forschung (BMBF) grant numbers: IFB/CCI: 01E01303 and E-med SysINFLAME: 012X1306F, 01GM1517C. The Deutsche Forschungsgemeinschaft (DFG, German Research Foundation) grant numbers: GR1617/8-1, IMPATH-SFB (SFB1160/1) and SFB 403222702 – SFB 1381 (Young Investigator Grant). The Kraft laboratory has received funding from the Deutsche Forschungsgemeinschaft (DFG, German Research Foundation) Project-IDs 450216812, 409673687, SFB 1381 (Project ID 403222702), SFB 1177 (Project ID 259130777), under Germany's Excellence Strategy (CIBSS - EXC-2189- Project ID 390939984) and from the European Research Council (ERC) under the European Union's Horizon 2020 research and innovation programme under grant agreement No 769065. This work reflects only the authors' view and the European Union's Horizon 2020 research and innovation programme is not responsible for any use that may be made of the information it contains.

Author contributions: LG-D and BG designed the study. LG-D, ES, LAL, MCD, PS, SN, SR, PM and AR performed the experiments. LG-D, LAL, ES, MCD, PS, SG, SJ, MP, KT, ER, AR, CM and CK analyzed and interpreted the data, LG-D and BG wrote the manuscript with contributions from all co-authors. LG-D, LAL, ES, MCD, PS, SN, SG, and AR prepared the figures. BG and LG-D secured funding for this work. All authors reviewed and approved the manuscript.

Conflict-of-interest disclosure: The authors declare no competing financial interests

Table 1: Predicted LRBA interactors by computational predictions

N°	Gen	Protein code	Protein	Function	Database
1	FBXW10	Q5XX13	F-box/WD repeat-containing protein 10	Ubiquitination and subsequent proteasomal degradation of target proteins	FuncBase
2	DCAF12L1	Q5VU92	DDB1-and CUL4-associated factor 12-like protein 1	Unknown	FuncBase
3	DCAF12L2	Q5VW00	DDB1-and CUL4-associated factor 12-like protein 2	Unknown	FuncBase
4	DOCK5	Q9H7D0	Dedicator of cytokenesis protein 5	Epithelial cell migration	FuncBase
5	GABARAP	O95166	GABA (A) receptor-associated protein l	Apoptosis and autophagy	STRING
6	GABARAPL 1	Q9H0R8	GABA (A) receptor-associated protein like 1	Formation of autophagosomal vacuoles	STRING
7	GABARAPL 3	Q9BY60	GABA (A) receptor-associated protein like 1	Formation of autophagosomes	STRING
8	GNB1L	Q9BYB4	Guanine nucleotide-binding protein subunit beta-like protein 1	Intracellular signal transduction	FuncBase
9	IFT80	Q9P2H3	Intraflagellar transport protein 80 homolog	Development and maintenance of motile and sensory cilia	FuncBase
10	KIAA1875	A6NE52	WD repeat-containing protein 97	Generation of catalytic spliceosome	FuncBase
11	KIF21A	Q7Z4S6	Kinesin-like protein KIF21A	Microtubule-based movement	FuncBase
12	LRRK2	Q5S007	Leucine-rich repeat serine/threonine-protein kinase	Autophagy through the CaMKK/AMPK	FuncBase
13	LYST	Q99698	Lysosomal-trafficking regulator	Sorting endosomal resident proteins into late multivesicular endosomes	FuncBase
14	MYL3	P08590	Myosin light chain 3	Actin monomer binding	STRING
15	NBEAL1	Q6ZS30	Neurobeachin-like protein 1	Phospholipid binding	FuncBase
16	NSMAF	Q92636	Protein FAN	Ceramide metabolic process	FuncBase
17	NUP214	P35658	Nuclear pore complex protein Nup214	Nuclear export signal receptor activity	FuncBase
18	PIK3R4	Q99570	Phosphoinositide 3-kinase regulatory subunit 4	Macroautophagy and late endosome to vacuole transport	FuncBase STRING
19	RBP3	P10745	Retinol- binding protein 3	Transport of the retinoids	STRING
20	SMN1	Q16637	Survival motor neuron 1	Assembly of small nuclear ribonucleoproteins	STRING
21	TLE6	Q9H808	Transducin-like enhancer protein 6	Positive regulation of neuron differentiation	FuncBase
22	VPS8	Q8N3P4	Vacuolar protein sorting-associated protein 8 homolog	Endosomal vesicle fusion	FuncBase
23	VPS11	Q9H270	Vacuolar protein sorting-associated protein 11 homolog	Vesicle-mediated protein trafficking	FuncBase
24	WDR88	Q6ZMY6	WD repeat-containing protein 88	Unknown	FuncBase

25	WDFY3	Q8IZQ1	WD repeat- and FYVE-containing protein 3	Aggrephagy	FuncBase
26	WDR46	O15213	WD repeat-containing protein 46	Scaffold component of the nucleolar structure	FuncBase
27	WDR87	Q6ZQQ6	WD repeat-containing protein 87	Unknown	FuncBase

List of the 28 potential LRBA interactors identified by FuncBase and/or STRING. Proteins are listed alphabetically. Proteins highlighted in grey were selected for validation by co-immunoprecipitations (Co-IP) shown in Figure 2 and supplementary Figure 1, or proximity ligation assay (PLA) shown in Figure 2 and supplementary Figure 2.

References

1. Cullinane, A.R., A.A. Schaffer, and M. Huizing, *The BEACH is hot: a LYST of emerging roles for BEACH-domain containing proteins in human disease.* Traffic, 2013. **14**(7): p. 749-66.
2. Gulsuner, S., et al., *Homozygosity mapping and targeted genomic sequencing reveal the gene responsible for cerebellar hypoplasia and quadrupedal locomotion in a consanguineous kindred.* Genome Res, 2011. **21**(12): p. 1995-2003.
3. Gunay-Aygun, M., et al., *NBEAL2 is mutated in gray platelet syndrome and is required for biogenesis of platelet alpha-granules.* Nat Genet, 2011. **43**(8): p. 732-4.
4. Shiflett, S.L., J. Kaplan, and D.M. Ward, *Chediak-Higashi Syndrome: a rare disorder of lysosomes and lysosome related organelles.* Pigment Cell Res, 2002. **15**(4): p. 251-7.
5. Lopez-Herrera, G., et al., *Deleterious mutations in LRBA are associated with a syndrome of immune deficiency and autoimmunity.* Am J Hum Genet, 2012. **90**(6): p. 986-1001.
6. Azizi, G., et al., *Clinical, immunologic, molecular analyses and outcomes of iranian patients with LRBA deficiency: A longitudinal study.* Pediatr Allergy Immunol, 2017. **28**(5): p. 478-484.
7. Kostel Bal, S., et al., *Multiple Presentations of LRBA Deficiency: a Single-Center Experience.* J Clin Immunol, 2017. **37**(8): p. 790-800.
8. Gamez-Diaz, L., et al., *The extended phenotype of LPS-responsive beige-like anchor protein (LRBA) deficiency.* J Allergy Clin Immunol, 2016. **137**(1): p. 223-230.
9. Alkhairy, O.K., et al., *Spectrum of Phenotypes Associated with Mutations in LRBA.* J Clin Immunol, 2016. **36**(1): p. 33-45.
10. Lo, B., et al., *AUTOIMMUNE DISEASE. Patients with LRBA deficiency show CTLA4 loss and immune dysregulation responsive to abatacept therapy.* Science, 2015. **349**(6246): p. 436-40.
11. Lo, B., et al., *CHAI and LATAIE: new genetic diseases of CTLA-4 checkpoint insufficiency.* Blood, 2016. **128**(8): p. 1037-42.
12. Jamee, M., et al., *Comprehensive comparison between 222 CTLA-4 haploinsufficiency and 212 LRBA deficiency patients: a systematic review.* Clin Exp Immunol, 2021. **205**(1): p. 28-43.
13. Mizushima, N., *Autophagy: process and function.* Genes Dev, 2007. **21**(22): p. 2861-73.
14. Dikic, I. and Z. Elazar, *Mechanism and medical implications of mammalian autophagy.* Nat Rev Mol Cell Biol, 2018. **19**(6): p. 349-364.

15. Schmid, D., M. Pypaert, and C. Munz, *Antigen-loading compartments for major histocompatibility complex class II molecules continuously receive input from autophagosomes.* Immunity, 2007. **26**(1): p. 79-92.
16. Cui, B., et al., *Autophagy and the Immune Response.* Adv Exp Med Biol, 2019. **1206**: p. 595-634.
17. Wu, Y., et al., *PI3P phosphatase activity is required for autophagosome maturation and autolysosome formation.* EMBO Rep, 2014. **15**(9): p. 973-81.
18. Pankiv, S., et al., *FYCO1 is a Rab7 effector that binds to LC3 and PI3P to mediate microtubule plus end-directed vesicle transport.* J Cell Biol, 2010. **188**(2): p. 253-69.
19. Pankiv, S. and T. Johansen, *FYCO1: linking autophagosomes to microtubule plus end-directing molecular motors.* Autophagy, 2010. **6**(4): p. 550-2.
20. Beaver, J.E., et al., *FuncBase: a resource for quantitative gene function annotation.* Bioinformatics, 2010. **26**(14): p. 1806-7.
21. Szklarczyk, D., et al., *The STRING database in 2017: quality-controlled protein-protein association networks, made broadly accessible.* Nucleic Acids Res, 2017. **45**(D1): p. D362-D368.
22. Koyasu, S., *The role of PI3K in immune cells.* Nat Immunol, 2003. **4**(4): p. 313-9.
23. Yan, Y., et al., *hVps15, but not Ca2+/CaM, is required for the activity and regulation of hVps34 in mammalian cells.* Biochem J, 2009. **417**(3): p. 747-55.
24. Ohashi, Y., S. Tremel, and R.L. Williams, *VPS34 complexes from a structural perspective.* J Lipid Res, 2019. **60**(2): p. 229-241.
25. Backer, J.M., *The intricate regulation and complex functions of the Class III phosphoinositide 3-kinase Vps34.* Biochem J, 2016. **473**(15): p. 2251-71.
26. Funderburk, S.F., Q.J. Wang, and Z. Yue, *The Beclin 1-VPS34 complex--at the crossroads of autophagy and beyond.* Trends Cell Biol, 2010. **20**(6): p. 355-62.
27. Axe, E.L., et al., *Autophagosome formation from membrane compartments enriched in phosphatidylinositol 3-phosphate and dynamically connected to the endoplasmic reticulum.* J Cell Biol, 2008. **182**(4): p. 685-701.
28. Nascimbeni, A.C., P. Codogno, and E. Morel, *Phosphatidylinositol-3-phosphate in the regulation of autophagy membrane dynamics.* FEBS J, 2017. **284**(9): p. 1267-1278.
29. Klionsky, D.J., et al., *Guidelines for the use and interpretation of assays for monitoring autophagy (4th edition)(1).* Autophagy, 2021. **17**(1): p. 1-382.
30. Matsui, T., et al., *Autophagosomal YKT6 is required for fusion with lysosomes independently of syntaxin 17.* J Cell Biol, 2018. **217**(8): p. 2633-2645.
31. Kim, D.H., et al., *mTOR interacts with raptor to form a nutrient-sensitive complex that signals to the cell growth machinery.* Cell, 2002. **110**(2): p. 163-75.
32. Sarbassov, D.D., et al., *Rictor, a novel binding partner of mTOR, defines a rapamycin-insensitive and raptor-independent pathway that regulates the cytoskeleton.* Curr Biol, 2004. **14**(14): p. 1296-302.
33. Chauvin, C., et al., *Ribosomal protein S6 kinase activity controls the ribosome biogenesis transcriptional program.* Oncogene, 2014. **33**(4): p. 474-83.
34. Hindupur, S.K., A. Gonzalez, and M.N. Hall, *The opposing actions of target of rapamycin and AMP-activated protein kinase in cell growth control.* Cold Spring Harb Perspect Biol, 2015. **7**(8): p. a019141.
35. Behrends, C., et al., *Network organization of the human autophagy system.* Nature, 2010. **466**(7302): p. 68-76.
36. Mackeh, R., et al., *Autophagy and microtubules - new story, old players.* J Cell Sci, 2013. **126**(Pt 5): p. 1071-80.

37. Munz, C., *The Macroautophagy Machinery in MHC Restricted Antigen Presentation.* Front Immunol, 2021. **12**: p. 628429.
38. Jain, B.P. and S. Pandey, *WD40 Repeat Proteins: Signalling Scaffold with Diverse Functions.* Protein J, 2018. **37**(5): p. 391-406.
39. Isakson, P., P. Holland, and A. Simonsen, *The role of ALFY in selective autophagy.* Cell Death Differ, 2013. **20**(1): p. 12-20.
40. Liu, X., et al., *The BEACH-containing protein WDR81 coordinates p62 and LC3C to promote aggrephagy.* J Cell Biol, 2017. **216**(5): p. 1301-1320.
41. Bilanges, B., Y. Posor, and B. Vanhaesebroeck, *PI3K isoforms in cell signalling and vesicle trafficking.* Nat Rev Mol Cell Biol, 2019. **20**(9): p. 515-534.
42. Johnson, E.E., et al., *Gene silencing reveals a specific function of hVps34 phosphatidylinositol 3-kinase in late versus early endosomes.* J Cell Sci, 2006. **119**(Pt 7): p. 1219-32.
43. Falasca, M. and T. Maffucci, *Rethinking phosphatidylinositol 3-monophosphate.* Biochim Biophys Acta, 2009. **1793**(12): p. 1795-803.
44. Gaullier, J.M., et al., *Interaction of the EEA1 FYVE finger with phosphatidylinositol 3-phosphate and early endosomes. Role of conserved residues.* J Biol Chem, 2000. **275**(32): p. 24595-600.
45. Marat, A.L. and V. Haucke, *Phosphatidylinositol 3-phosphates-at the interface between cell signalling and membrane traffic.* EMBO J, 2016. **35**(6): p. 561-79.
46. Polson, H.E., et al., *Mammalian Atg18 (WIPI2) localizes to omegasome-anchored phagophores and positively regulates LC3 lipidation.* Autophagy, 2010. **6**(4): p. 506-22.
47. Dooley, H.C., et al., *WIPI2 links LC3 conjugation with PI3P, autophagosome formation, and pathogen clearance by recruiting Atg12-5-16L1.* Mol Cell, 2014. **55**(2): p. 238-52.
48. Bilanges, B., et al., *Vps34 PI 3-kinase inactivation enhances insulin sensitivity through reprogramming of mitochondrial metabolism.* Nat Commun, 2017. **8**(1): p. 1804.
49. Chen, J., et al., *Mutations in FYCO1 cause autosomal-recessive congenital cataracts.* Am J Hum Genet, 2011. **88**(6): p. 827-838.
50. Mrakovic, A., et al., *Rab7 and Arl8 GTPases are necessary for lysosome tubulation in macrophages.* Traffic, 2012. **13**(12): p. 1667-79.
51. Pu, J., et al., *Mechanisms and functions of lysosome positioning.* J Cell Sci, 2016. **129**(23): p. 4329-4339.
52. Li, Y., et al., *Decoding three distinct states of the Syntaxin17 SNARE motif in mediating autophagosome-lysosome fusion.* Proc Natl Acad Sci U S A, 2020. **117**(35): p. 21391-21402.
53. Cabrera, M., et al., *The Mon1-Ccz1 GEF activates the Rab7 GTPase Ypt7 via a longin-fold-Rab interface and association with PI3P-positive membranes.* J Cell Sci, 2014. **127**(Pt 5): p. 1043-51.
54. Pengo, N. and S. Cenci, *The role of autophagy in plasma cell ontogenesis.* Autophagy, 2013. **9**(6): p. 942-4.
55. Pengo, N., et al., *Plasma cells require autophagy for sustainable immunoglobulin production.* Nat Immunol, 2013. **14**(3): p. 298-305.
56. Clarke, A.J., et al., *B1a B cells require autophagy for metabolic homeostasis and self-renewal.* J Exp Med, 2018. **215**(2): p. 399-413.
57. Arbogast, F., et al., *ATG5 is required for B cell polarization and presentation of particulate antigens.* Autophagy, 2019. **15**(2): p. 280-294.
58. Gamez-Diaz, L., et al., *Immunological phenotype of the murine Lrba knockout.* Immunol Cell Biol, 2017. **95**(9): p. 789-802.

59. Willinger, T. and R.A. Flavell, *Canonical autophagy dependent on the class III phosphoinositide-3 kinase Vps34 is required for naive T-cell homeostasis.* Proc Natl Acad Sci U S A, 2012. **109**(22): p. 8670-5.
60. Wang, K.W., et al., *Enhanced susceptibility to chemically induced colitis caused by excessive endosomal TLR signaling in LRBA-deficient mice.* Proc Natl Acad Sci U S A, 2019. **116**(23): p. 11380-11389.
61. Huang, K. and D.C. Fingar, *Growing knowledge of the mTOR signaling network.* Semin Cell Dev Biol, 2014. **36**: p. 79-90.
62. Magnuson, B., B. Ekim, and D.C. Fingar, *Regulation and function of ribosomal protein S6 kinase (S6K) within mTOR signalling networks.* Biochem J, 2012. **441**(1): p. 1-21.
63. Egan, D.F., et al., *Phosphorylation of ULK1 (hATG1) by AMP-activated protein kinase connects energy sensing to mitophagy.* Science, 2011. **331**(6016): p. 456-61.
64. Brachmann, S., et al., *PI3K and mTOR inhibitors: a new generation of targeted anticancer agents.* Curr Opin Cell Biol, 2009. **21**(2): p. 194-8.
65. Goodman, M., et al., *AMPK Activators as a Drug for Diabetes, Cancer and Cardiovascular Disease.* Pharm Regul Aff, 2014. **3**(2).
66. Azizi, G., et al., *New therapeutic approach by sirolimus for enteropathy treatment in patients with LRBA deficiency.* Eur Ann Allergy Clin Immunol, 2017. **49**(5): p. 235-239.
67. Seidel, M.G., et al., *Treatment of severe forms of LPS-responsive beige-like anchor protein deficiency with allogeneic hematopoietic stem cell transplantation.* J Allergy Clin Immunol, 2018. **141**(2): p. 770-775 e1.

Figure legends

Figure 1. LRBA interacts with PIK3R4 through its WD40 domain. A) *In silico* identification of LRBA interaction protein network using FuncBase (left) and STRING version 10 (middle). In STRING, colored lines indicate evidence of neighborhood (green), concurrence (blue), coexpression (black), experimental evidence (purple) and fusion (red). Gene Ontology (GO) enrichment analysis (right) of 28 potential interactors of LRBA was conducted for the three main GO domains cellular compartment. The length of the bar represents the log10 Benjamini-Hochberg corrected p-value. The numbers represent the percentage of associated genes for each biological process. B) LRBA interacts with phosphoinositide 3-kinase regulatory subunit 4 (PIK3R4) shown by proximity ligation assay (PLA) on healthy control LCL cells. PLA signal is absent in LCL cells from a LRBA-deficient patient. Nuclear DAPI staining is shown in blue and the LRBA-PIK3R4 interaction is shown as a red signal. Scale bars, 20 µm. C) Dots (PLA signal) per cell were quantified in 50 cells per experiment using Duolink Image tool (SIGMA). A t-test was applied from two independent experiments, ***$p<0.001$. D) WT HEK293T cells were transfected with his-tagged PIK3R4 and with myc-LRBA plasmid. Pull down (IP) was performed with anti-LRBA and immunoblotted (IB) with anti-PIK3R4. E) LRBA-PIK3R4 interaction occurs *via* WD40 domain. Schematic representation of the different flag-tagged LRBA plasmids containing the

different LRBA protein domains. Each fragment is marked with an asterisk and their corresponding molecular weight are F1: 43 kDa, F2: 65 kDa, F3: 75 kDa, F4: 20 kDa, F5: 68 kDa, F6: 59 kDa, and F7: 31 kDa. HEK293T cells were transfected with his-tagged PIK3R4 and flag-tagged protein fragments 1 to 7 of LRBA. Flag-LRBA immunoprecipitates (IP) from transfected cells were immunoblotted with anti-PIK3R4. F) Ratio of PIK3R4/LRBA fragment was calculated for n=3 independent experiments. A t-test was applied, **p<0.005. G) Models of the WD40 domains of PIK3R4 (light green) and LRBA (purple). The inserted repeat propeller of LRBA is shown in cyan. H) Model of the complex of LRBA (purple) with PIK3R4 (light green)/PIK3C3 (VPS34, silver). The inserted repeat propeller of LRBA-WD40 is shown in cyan.

Figure 2. Proper function of the PI3K-III complex requires LRBA. A) Schematic representation of PI3K-III complex activity at the initiation of autophagosome formation. B) Production of PI(3)P was measured in lipid extracts of LRBA-KO HEK293T cells (red) under basal conditions, or upon treatment with 333 nM of Torin 1 alone (autophagy inducer), or in combination with 1nM of VPS34-IN1 (PI3K-III complex inhibitor) for 4 hours. PI(3)P production was measured in duplicates for n=3 independent experiments. A t-test was applied, **p-value <0.01. C) Reduced DFCP-1 and WIPI2 recruitment in LRBA-KO HEK293T cells. Representative confocal microscopy images of WT and LRBA-KO HEK293T cells stained with anti-DFCP-1 (green) or anti-WIPI2 (red) antibody after incubation for one hour with control medium, 50 µM Rapamycin, 333 nM Torin1, EBSS or 100 nM Wortmannin. Scale bar 5 µM D-E). The number of dots per cell was assessed using ImageJ for D) 89 to 200 nuclei from WT cells (blue) or LRBA-KO HEK293T cells (red) and E) 51 to 70 nuclei from WT (blue) or LRBA-KO HEK293 cells (red). The statistical analysis was performed using a Two-way ANOVA: ****p-values < 0.0001. F) Representative confocal microscopy images of WT and LRBA-KO HEK293T cells stained with anti-DFCP-1 antibody after treatment with the indicated concentrations of VPS34-IN1 for one hour followed by one hour incubation with 333 nM Torin1. E) The number of dots per cell was assessed using ImageJ for 29 to 110 nuclei from WT (blue) or LRBA-KO HEK293T cells (red). The statistical analysis was performed using a Two-way ANOVA: ****p-values < 0.0001. Scale bar 5 µM and n = 3 experiment.

Figure 3. LRBA deficiency leads to impaired autophagic flux due to blockage of autophagosome-lysosome fusion. A) Representative confocal microscopy images on WT and LRBA-KO HEK293T cells stably transduced with mCherry-GFP-LC3 tandem vector after 4 h treatment with 200 nM Bafilomycin A1 alone, 333 nM Torin1 alone, or in a combination of both. B) Ratio red/green dots counted with ImageJ in 85 nuclei from WT (blue) and 79 nuclei from LRBA-KO HEK293T (red) in three different experiments. Statistical analysis was performed using a Two-

way ANOVA. C) Representative immunoblot analysis of the expression of p62 relative to the housekeeping protein GAPDH in WT and LRBA-KO HEK293T cells at basal conditions or after 4 h stimulation with 333 nM Torin1 alone, with 200 nM Bafilomycin A1 alone, or with a combination of both. D) Densitometry analysis of p62 immunoblots (n=3 per condition) showing p62 accumulation in LRBA-KO cells. E-G) Measurement with Imaris 9.7 of the diameter (in µm) of 50 autophagosomes in mCherry-GFP-LC3 transduced HEK293T cells (E), and of 68 autophagosomes detected at endogenous levels in HEK293T cells using anti-LC3 antibody (F-G) upon Bafilomycin stimulation. LRBA-KO cells (red) showed enlarged autophagosomes in both conditions in comparison to WT cells (blue). The statistical analysis was performed using Welch´s test p=0.0017 (**). The dashed lines represent the mean and the dot lines represent the first and third quartiles

Figure 4. Absence of LRBA leads to an accumulation of abnormal, sealed and unfused autophagosomes and hyperactivation of mTOR signaling. A) Schematic illustration of the protease protection assay. Cell homogenates are treated with proteinase K resulting in the degradation of exposed proteins including p62 but not of membrane-enclosed proteins. B) HEK293T WT and LRBA-KO cells were grown in EBSS medium with 300 nM Torin 1 for 2 h. After lysis, cell membranes were subjected to proteinase K and Triton X-100 treatment as indicated and analyzed by anti-p62 Western blotting. C) Quantification of three independent biological replicates of the protease assay. The mean ± SEM is shown. Statistical analysis was performed using Welch's t-test *p<0.05. D) Accumulation of autophagosomes in absence of LRBA. WT and LRBA-KO HEK293T cells were grown in EBSS medium with 300 nM Torin1 for 3 h with or without 200 nM Bafilomycin A1, and cell homogenates were subjected to OptiPrep flotation analysis. The asterisk indicates the accumulation of autophagosomes in LRBA-KO homogenates. E) Electron microscopy images on LPS-stimulated B cells from wild-type and *Lrba-/-* mice using immunogold labeling for LC3. Arrows point to autophagosomes, N: nucleus, M: mitochondria. Images represent higher magnification of the inset's black-boxed area. A total of three mice per genotype were analyzed. F-G) Immunoblot analyses showing increased expression of pS6K in LRBA-deficient cells. F) Representative immunoblot analysis of LRBA, S6K total, S6K pT389, AMPK total, AMPK pT172 and GAPDH were performed in (left) LCL lysates from a healthy donor and a LRBA-deficient patient, and in (right) shControl and shLRBA-HeLa cells at basal conditions. G) Bar graphs represent densitometry analysis of protein expression from LCL and HeLa cells using ImageJ. Quantifications of protein expression were previously normalized to GAPDH and to healthy donor sample or shControl (dotted line). The histograms represent the means ± S.D. obtained from three different blots **P<0.001 (Mann-Whitney).

Figure 5. LRBA-FYCO interaction facilitates autophagosome mobilization and lysosome positioning A) Mobility of autophagosomes was evaluated by time-lapse movies (supplementary video 1 and 2) acquired from individual frames, color-coded and projected into one image, using the temporal color-coding module of the Zeiss Zen Black software. B) Quantification of autophagosomes velocity was performed using Manual Track. Each dot corresponds to one autophagosome tracked over at 25 frames for shControl (blue) and shLRBA HeLa cells (red). Bars represent Mean ± SD (n=4). Statistical analysis was performed using Welch´s t-test. C) Correlation graph of velocity and area of the autophagosomes tracked in shControl (blue) and shLRBA HeLa cells (red). D) Lysosomes from shControl (blue) and shLRBA (red) HeLa cells under basal conditions were stained with LysoTracker red. shLRBA HeLa cells showed cytosolic spread-out of lysosomes in comparison to perinuclear lysosomal distribution in the shControl cells. E) Representative fluorescent microscopy images of WT and shLRBA cells either stained with anti-TEFB antibody and GFP-coupled secondary (top) or transfected with a TFEB-GFP-containing vector (bottom) upon resting conditions showing normal biogenesis of lysosomes in absence of LRBA**.** F) Electron microscopy images on LPS-stimulated B cells from wild-type and *Lrba-/-* mice using immunoperoxidase labeling for Lamp-1. Arrows point to lysosomes. N: nucleus, M: mitochondria. Images represent higher magnification of the inset's black-boxed area. A total of three mice per genotype were analyzed. G) WT HEK293T cells were transfected with DNA encoding FYCO1-GFP and/or myc-LRBA plasmid. Pull down was performed with anti-LRBA and immunoblotted with anti-GFP. H) Interaction of LRBA and FYCO-1 occurs *via* BEACH domain (fragment 6). WT HEK293T cells were transfected with DNA encoding FYCO1-GFP plasmid and flag-tagged fragments 1 to 7 of LRBA. Flag-LRBA immunoprecipitates from transfected cells were immunoblotted with anti-GFP. Representative experiment from two independent experiments. The bar graph (right) represent the relative Flag expression normalized to GFP measured in the different LRBA-fragments.

Figure 6: Loss of LRBA leads to enhanced CD4$^+$ T cell activation as a consequence of increased MHC class II restricted antigen presentation. A) Schematic illustration of the antigen presentation assay. WT or LRBA-KO HaCat cells stably expressing GFP-LC3 or MP1-LC3 (target cells), and pre-treated with IFN-γ for 24h to up-regulate MHC class II molecules were cultured with a MP1-specific CD4$^+$ T-cell clone (effector cells) from a healthy donor for 20 h. Following incubation, proinflammatory cytokines were measured in the culture supernatants. B-E) ELISA assays on culture supernatants from co-cultures of an T cell effector to HaCat target cell (E:T=10:5) ratios as described in A. Scatter plots represent the IFN-γ (n=4), MIP-1β (n=4), TNFα

(n=2) and IL-6 (n=4) secretion and each symbol represents a biological replicate. Ratio paired student t-test, Two-tailed: p*<0.05, **<0.0005. F) Representative confocal microscopy images of HaCat cells stimulated overnight with IFN-γ that were treated with 20 µM chloroquine for 6 h. Fixed cells were immunostained for HLA-DR (green), LC3 (red) and DAPI (blue) for the nuclei and then acquired using a SP8 Falcon confocal microscope (Leica), scale bar 5 µM. G) Graph represents the percentage of $LC3^{+}$ dots also positive for HLA-DR per cell (left) and the right panel shows the percentage of HLA-DR dots also positive for LC3 per cell with more than 30 cells quantified per condition. Unpaired t-test. Quantification of LC3, HLA-DR or double positive dots per cell was performed using a semiautomatic plugin designed on FIJI. The violin blot shows the average size in µM (H) or the number (I) of dots positive for HLA-DR per cell with more than 30 cells quantified per condition. Statistical analysis was performed using unpaired t-test.

Figure 1. LRBA interacts with PIK3R4 through its WD40 domain

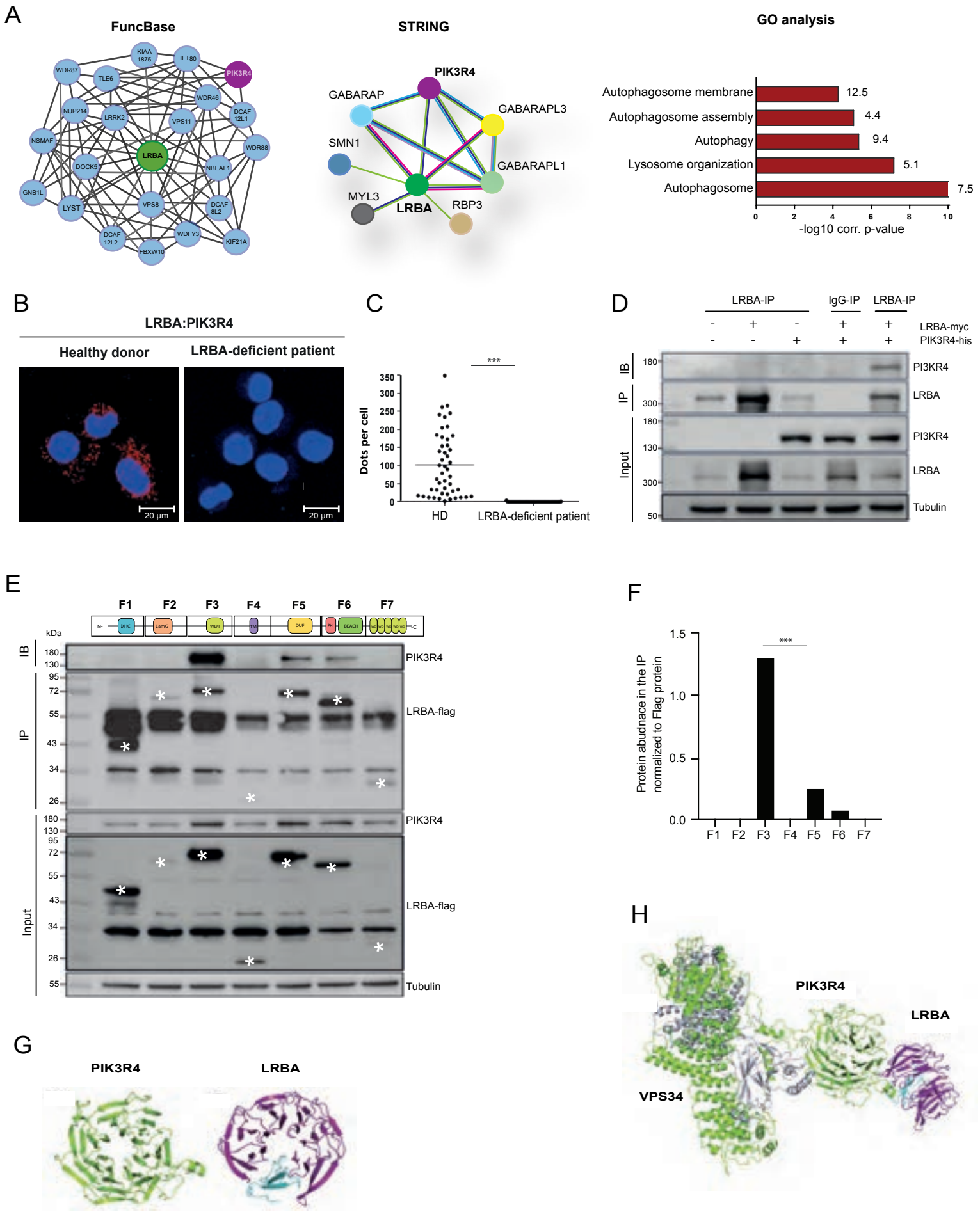

Figure 2. Proper function of the PI3K-III complex requires LRBA

A

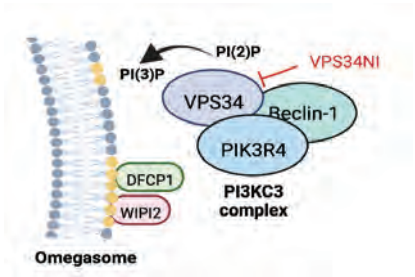

B

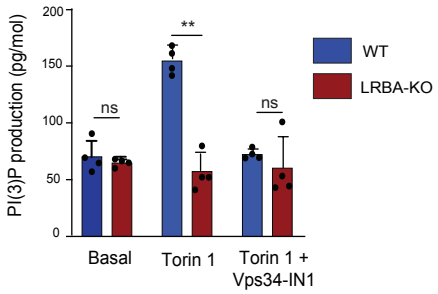

C

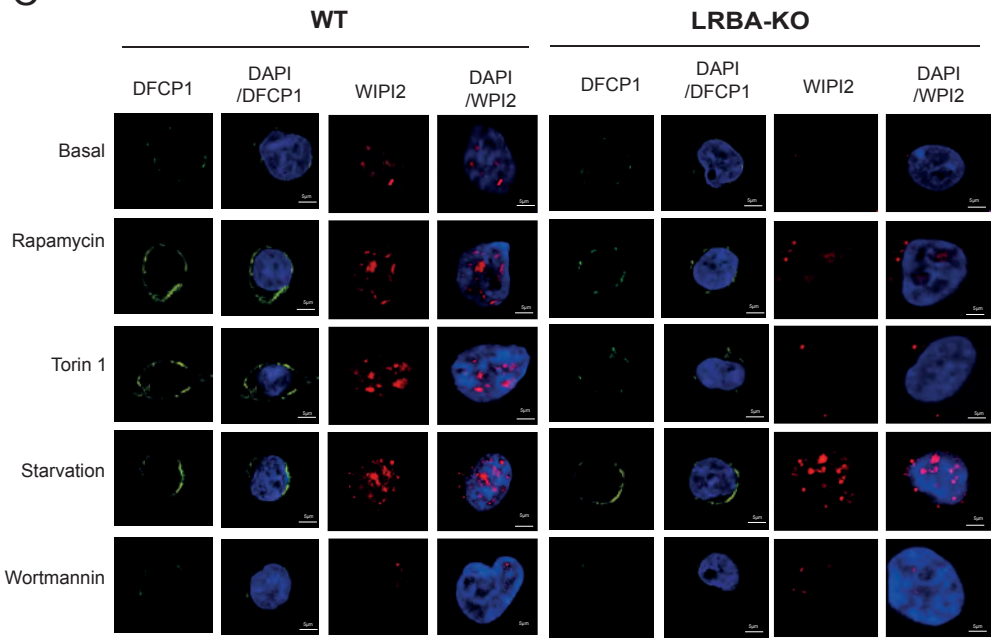

D

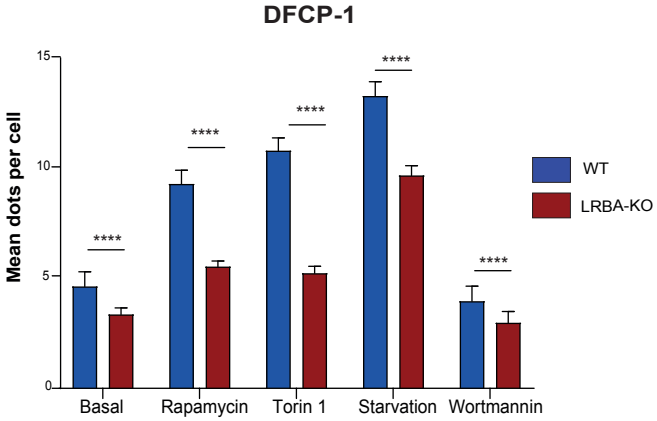

E

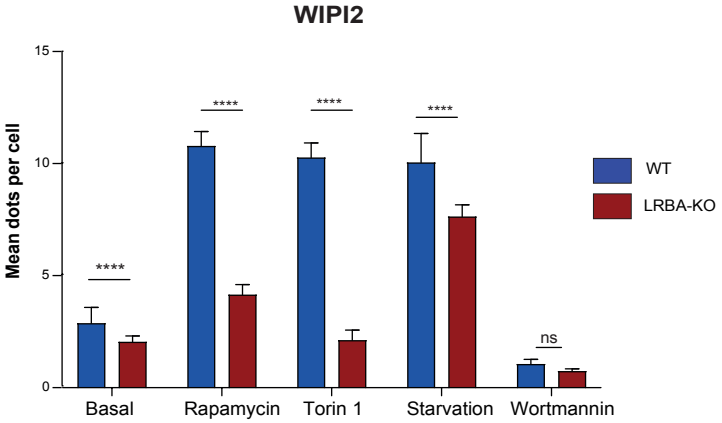

F

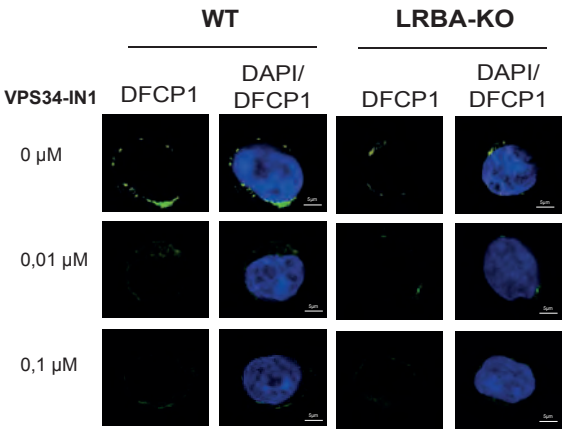

G

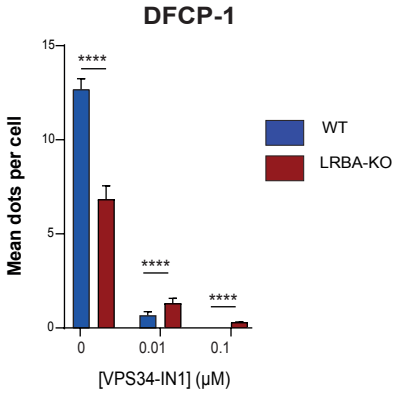

Figure 3. LRBA deficiency leads to impaired autophagic flux due to blockage of autophagosome-lysosome fusion.

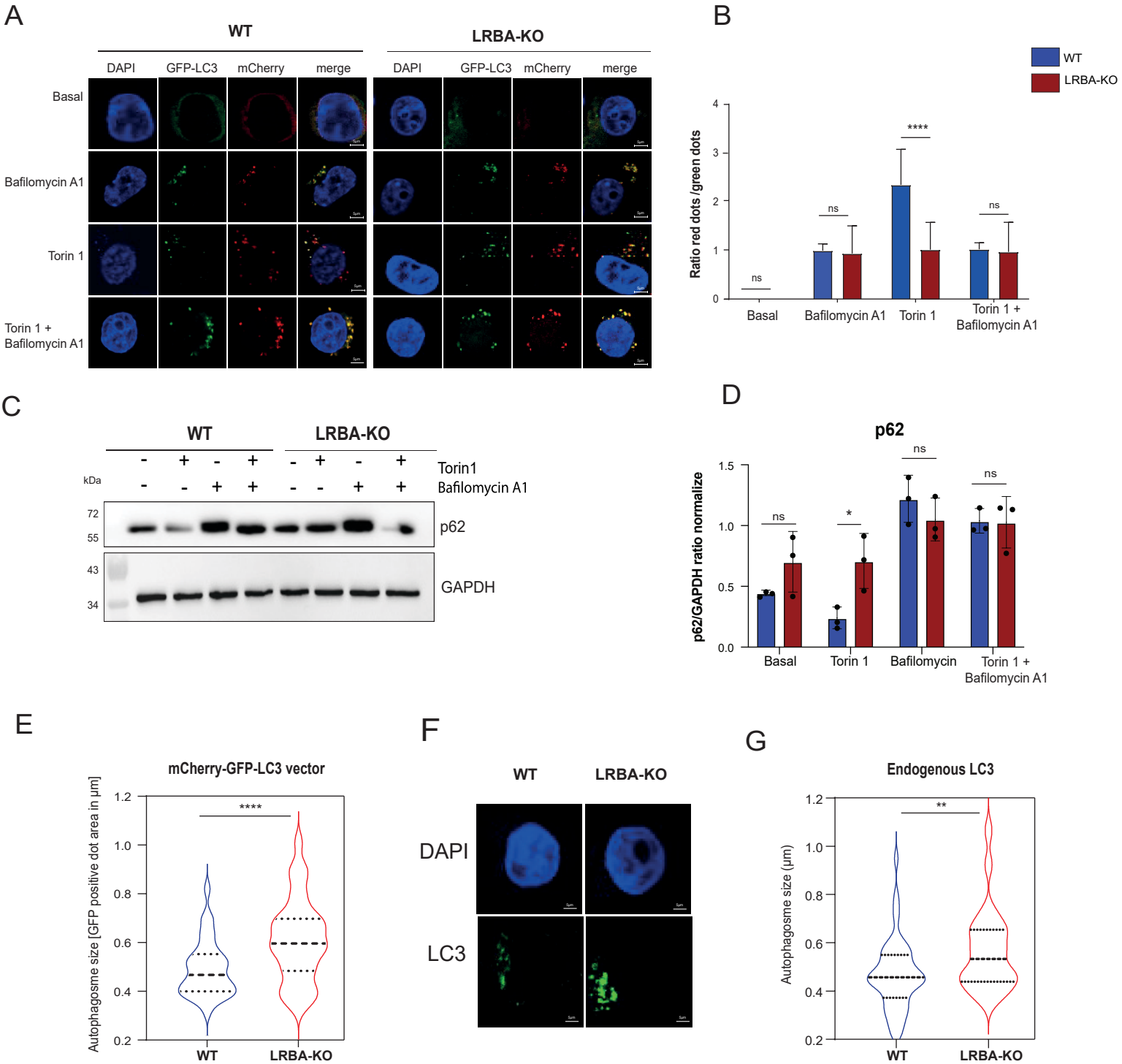

Figure 4. Absence of LRBA leads to an accumulation of abnormal, sealed and unfused autophagosomes

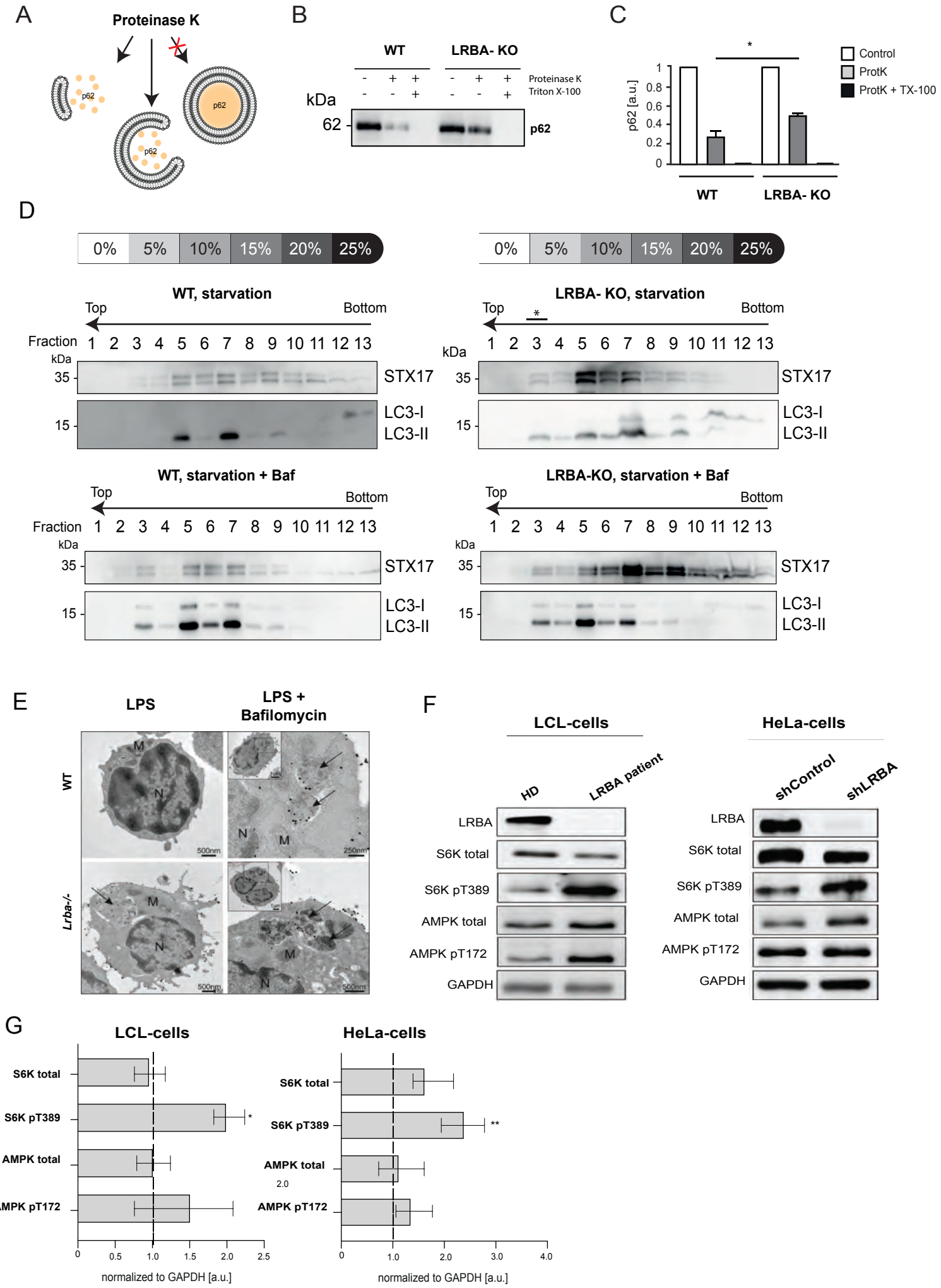

Figure 5. LRBA-FYCO interaction facilitates autophagosome mobilization and lysosome positioning

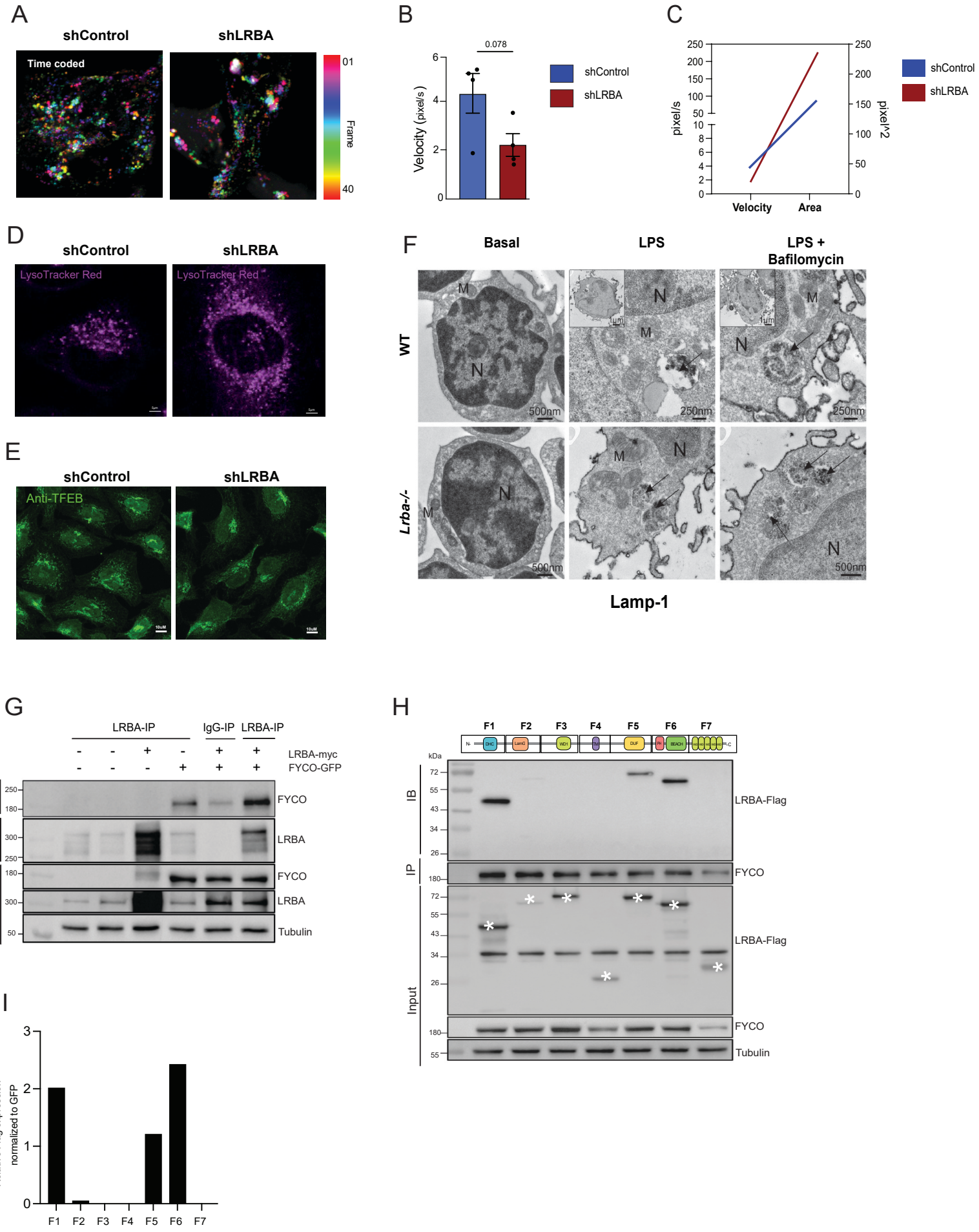

Figure 6. Loss of LRBA leads to enhanced T-cell activation as a consequence of increased antigen presentation

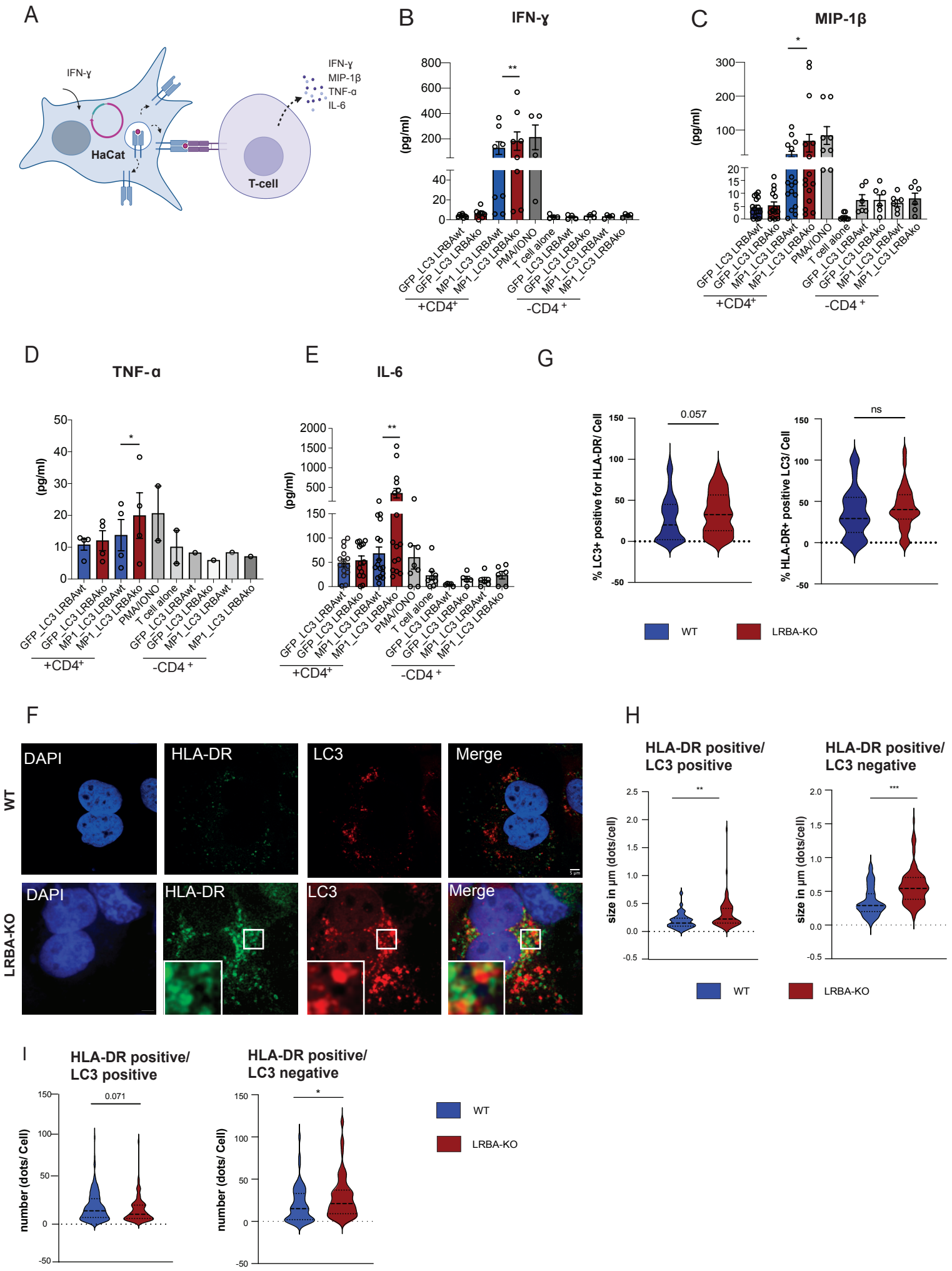
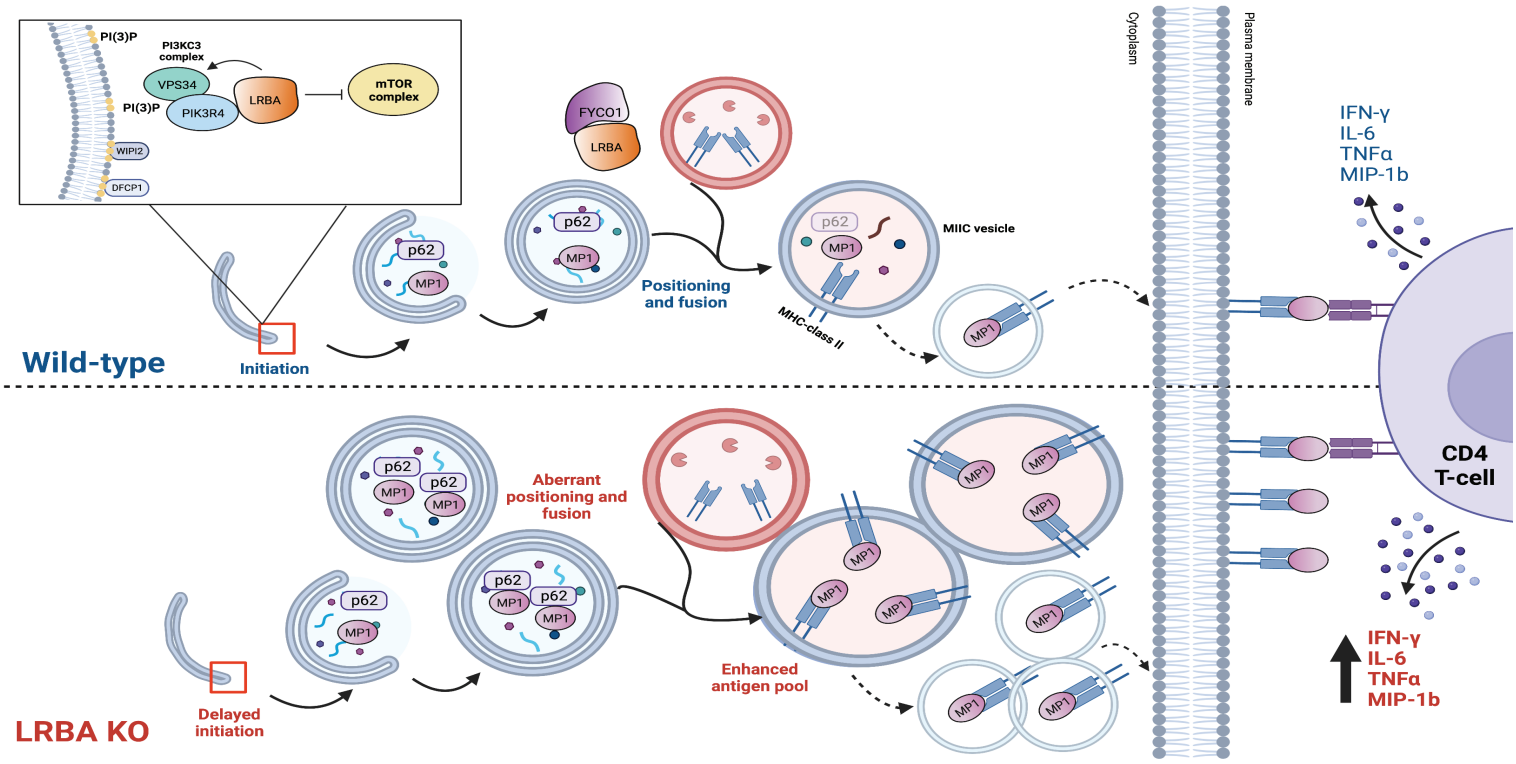
Graphical Abstract